NASA TM X-608

TECHNICAL MEMORANDUM

X-608

EFFECTS OF SEVERAL NOSE AND VERTICAL-FIN MODIFICATIONS ON THE LOW-ANGLE-OF-ATTACK STATIC STABILITY OF A WINGED REENTRY VEHICLE AT MACH NUMBERS OF 9.6 IN AIR AND 17.8 IN HELIUM

By Charles L. Ladson

Langley Research Center
Langley Air Force Base, Va.

NATIONAL AERONAUTICS AND SPACE ADMINISTRATION
WASHINGTON
November 1961

NATIONAL AERONAUTICS AND SPACE ADMINISTRATION

TECHNICAL MEMORANDUM X-608

EFFECTS OF SEVERAL NOSE AND VERTICAL-FIN MODIFICATIONS ON THE LOW-ANGLE-OF-ATTACK STATIC STABILITY OF A WINGED REENTRY VEHICLE AT MACH NUMBERS OF 9.6 IN AIR AND 17.8 IN HELIUM*

By Charles L. Ladson

SUMMARY

An investigation has been carried out in the Langley 11-inch hypersonic tunnel to study the effects of several nose, vertical-fin, and body-flap modifications on the low-angle-of-attack static stability characteristics of a winged reentry vehicle. From an analysis of the data, it is noted that configurations with slender bodies which are inboard of the wing leading edge in the apex region generally have longitudinal stability at low and zero angles of attack. However, configurations with bodies which extend to the wing leading edge near the nose generally have longitudinal instability in the same angle-of-attack range. Modification of the noses to include various canopy shapes had little effect on the stability.

Adding very blunt leading edges to the vertical fins reduced the angle-of-attack range over which the configuration was unstable, but increased the nonlinear moment characteristics about all three axes.

The use of an upper-surface body flap located toward the rear of the body proved to be the most successful method of providing longitudinal stability for the more blunt-nose configuration at low angles of attack. By use of the flap, the vehicle was stable at all angles of attack tested with little or no effect on either longitudinal performance or lateral and directional stability.

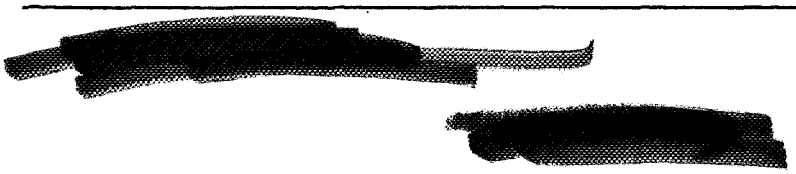

INTRODUCTION

Although winged reentry vehicles are contemplated as operating in the angle-of-attack range from the angle of attack for maximum lift (about 60°) to the angle of attack for maximum lift-drag ratio (about 15°), considerable interest has been shown in having the vehicle statically stable at angles of attack below that for maximum lift-drag ratio. Operation at these low angles of attack would probably be an emergency operating condition since the upper surfaces of the wing and body would be exposed to the airstream and thus would encounter much higher heating rates than when shielded at higher angles of attack. Vehicles currently under consideration do not have heat-protection materials on these surfaces sufficient to maintain low-angle-of-attack flight for more than a very few minutes at most, and the main aerodynamic problem is to return the vehicle to higher angles as rapidly as possible.

Typical winged reentry vehicles, as seen in references 1, 2, and 3, are noted generally to be unstable and to have very low flap effectiveness at angles of attack below about 15° at hypersonic speeds. However, if a vehicle has a large positive pitching moment (as is the case for the configuration shown in ref. 2) and enters the low-angle-of-attack region of instability, it would probably return to higher angles of attack. With the low flap effectiveness, however, vehicles with a very low positive or a negative pitching moment at low angles of attack may not be able to recover to higher angles, even with the use of negative elevon deflection (which further decreases the stability). Reference 3 also shows that the geometry of the vehicle nose has a strong influence on the low-angle-of-attack stability.

The purpose of the present investigation was to determine the effects of various nose, vertical-fin, and body-flap modifications on the low-angle-of-attack longitudinal, directional, and lateral stability. Tests were conducted in the Langley 11-inch hypersonic tunnel at Mach numbers of 9.6 with air as the test medium and 17.8 with helium as the test medium. Longitudinal performance and stability tests were conducted at angles of attack from -5° to 25°, while directional and lateral stability tests were made only at angles of attack of 0° and 10°.

SYMBOLS

All longitudinal performance data are referred to the stability axis system, while the directional, lateral, and longitudinal stability results are referred to the body axes.

b	span
$\bar{c}$	mean aerodynamic chord
C_D	drag coefficient
C_l	rolling-moment coefficient, $\frac{\text{Rolling moment}}{qSb}$
C_L	lift coefficient, $\frac{\text{Lift}}{qS}$
C_m	pitching-moment coefficient, $\frac{\text{Pitching moment}}{qS\bar{c}}$
C_n	yawing-moment coefficient, $\frac{\text{Yawing moment}}{qSb}$
C_N	normal-force coefficient, $\frac{\text{Normal force}}{qS}$
C_Y	side-force coefficient, $\frac{\text{Side force}}{qS}$
L/D	lift-drag ratio
$(L/D)_{max}$	maximum lift-drag ratio
M	Mach number
q	dynamic pressure
r	radius
S	planform area
α	angle of attack, deg
β	angle of sideslip, deg
φ	fin rollout angle, deg
δ_F	flap deflection, deg

MODELS AND DESIGNATIONS

Drawings showing the dimensions of the configurations and components tested are presented in figure 1. The various models and components are designated by letter symbols and subscripts and are identified as follows:

B_1, B_2 body shapes shown in figures 1(a) and 1(b), respectively

N_1 nose shape shown in figure 1(a) with three variations - N_{1A}, N_{1B}, and N_{1C}

N_2 nose shape shown in figure 1(b) with four variations - N_{2A}, N_{2B}, N_{2C}, and N_{2D}

W_1 wing, shown in figure 1(a)

V_o fairing block used with vertical fins off

V_1 55.5° swept vertical fins, individual fins are designated as V_{1L} (left fin) and V_{1R} (right fin)

V_2 50.2° swept vertical fins with thick leading edge

V_3 55.5° swept vertical fins with larger area than V_1

F_1 body flap

The models were constructed of aluminum with steel vertical fins and body flaps. The lower surface of the wing was flat, and the nose incidence was fixed at an angle of 4°. The vehicles incorporated wedge-slab-section wing-tip fins to provide directional stability. The model nose was blunted to a radius of 0.120 inch, and the leading edge of the wing had a radius of 0.052 inch (section taken normal to the wing leading edge). Photographs of several of the configurations tested are shown in figure 2.

The coefficients presented are based on wing planform area, span, and mean aerodynamic chord. The moment center is located at $0.43\bar{c}$ and $0.108b$ above the wing lower surface (fig. 1). The model constants are as follows:

$S = 12.490$ square inches

$b = 3.690$ inches

$\bar{c} = 4.064$ inches

APPARATUS, TESTS, AND PROCEDURE

Data contained herein were obtained in the Langley 11-inch hypersonic tunnel at $M = 9.6$ with air as the test medium and at $M = 17.8$ with helium as the test medium. At $M = 9.6$, the stagnation pressure was about 46 atmospheres, the stagnation temperature was 1,600° R, and the Reynolds number per inch was about 0.1×10^6. At $M = 17.8$ (in helium) the stagnation pressure was about 68 atmospheres, the stagnation temperature was 500° R, and the Reynolds number per inch was about 0.45×10^6. A calibration of the $M = 9.6$ air nozzle is contained in reference 4, while a description and a calibration of the $M = 17.8$ helium nozzle are contained in appendix A of reference 5 and in reference 6.

All tests were made with the use of a 6-component water-cooled strain-gage balance. The angles of attack of the model were measured optically by use of a light beam reflected from the model onto a calibrated scale. This method gave the true angle of attack of the model, including the deflection of the model and sting under load. Base-pressure measurements were made at $M = 9.6$, and the corrections were found to be negligible in comparison with the measured axial force. No corrections to the data therefore have been made for base pressure.

RESULTS AND DISCUSSION

Typical schlieren flow photographs showing the effects of nose shape, sideslip angle, fin rollout, and Mach number on the model shock pattern are shown in figures 3, 4, and 5. The longitudinal performance characteristics (variation of C_L, C_D, and L/D with α) and the longitudinal stability characteristics (variation of C_m with C_N) are presented in figures 6 to 12. The directional and lateral stability characteristics (C_l, C_n, and C_Y plotted against β at an angle of attack of 0°) are presented in figures 13 to 17, with the effect of each of the V_1 vertical fins, V_{1L} and V_{1R}, being shown in figure 15. Directional and lateral aerodynamic characteristics at an angle of attack of 10° are given in figures 18 and 19.

Longitudinal Performance and Stability

Effects of nose shape.- In figure 6 it is seen that changes in either nose or canopy shape have little effect on the performance characteristics of the configuration. As seen in figure 7, however, nose shape has an appreciable effect on the stability characteristics of the configuration at low angles of attack. Nose N_2, which extends outboard to the wing leading edge, produces a configuration which is unstable at angles of attack below about 5° whereas the N_1 nose, which is inboard of the wing leading edge, enables the configuration to be stable at all angles of attack. These trends are the same as were noted in reference 3. Breaking the continuity of the nose section to provide a windshield (noses N_{1B}, N_{1C}, N_{2B}, N_{2C}, and N_{2D}) decreases the stability in all cases as a result of the increased loading on the nose. However, this effect is not as severe as that encountered in the change between noses N_1 and N_2.

Effects of vertical fins.- Adding the vertical fins V_1 to both configurations $W_1N_{1A}B_1$ and $W_1N_{2C}B_2$ increased the drag coefficient as would be expected and reduced the lift as seen in figure 8. This loss in lift at angles of attack below about 15° is not only due to the vertical fins' inducing a high pressure on the wing upper surface as was noted in reference 7 but also to the force on the tail leading edge. This high pressure area along with the tail drag creates a nose-up or positive pitching-moment increment as seen in figure 9 with only a slight change in stability. The same trends are noted at both $M = 9.6$ in air and $M = 17.8$ in helium, although the coefficients are slightly different at $M = 17.8$ because of differences in Mach number and Reynolds number as well as differences due to using helium as the test medium.

One attempt at providing stability to configuration $W_1N_{2C}B_2V_1$ at angles of attack below about 10° was to increase the leading-edge radius of the vertical fins so that the resulting fins, V_2, would have much higher drag force and would probably create a higher pressure on the wing upper surface than fins V_1 as a result of the stronger bow shock. As seen in figures 9(b) at $M = 9.6$ and 9(d) at $M = 17.8$, the resulting configuration was still unstable at angles of attack below about 5°, and the pitching moment was more nonlinear than for the configuration with the V_1 fins. The $(L/D)_{max}$ of this configuration was not changed appreciably by the more blunt fin (figs. 8(c) and 8(d)).

The V_3 fins, which are larger in area but similar in shape to the V_1 fins, were added to increase the directional stability of configuration $W_1N_{2C}B_2V_1$. As shown in figures 8(c) and 8(d), no significant

effects on the longitudinal performance characteristics were noted with the change from the V_1 to the V_3 fins, and only a small positive pitching-moment increment was incurred as a result of the slightly higher axial force due to the V_3 fins (figs. 9(b) and 9(d)).

Effects of vertical-fin rollout.- The V_3 fins on configuration $W_1N_{2C}B_2$ were tested with $\varphi = 0^\circ$ and $\varphi = 20^\circ$. The purpose of rolling the fins out is to increase the directional stability at hypersonic speeds at angles of attack near that for maximum lift. Figure 10 indicates that the rolled out fins generate lift, and therefore a nose-down or negative pitching-moment increment results as seen in figure 12(a). This negative pitching-moment increment is nearly constant at angles of attack from 5° to 25° and would probably still exist at higher angles of attack. Although these fins do produce a moment increment, no significant changes in the overall stability occur.

Effects of body flap.- The use of a body flap located rearward on the body upper surface proved to be the most effective means of providing low-angle-of-attack longitudinal stability for configuration $W_1N_{2C}B_2V_1$. As seen in figure 12(b), the flap with $\delta_F = 60^\circ$ provided stability and positive pitching moment at $\alpha = 0^\circ$ for the configuration in the critical angle-of-attack range (α below 15°). Although a negative increment in lift and increased drag were incurred by use of the body flap, these effects were confined to the low angle-of-attack range so that the value of $(L/D)_{max}$ was not affected. (See fig. 11.)

Directional and Lateral Aerodynamic Characteristics at an Angle of Attack of 0°

Effects of nose shape.- Adding various canopy shapes to the two nose shapes had little effect on either the directional or the lateral aerodynamic characteristics presented in figure 13 for a Mach number of 9.6. Both noses N_1 and N_2 have very low or essentially zero directional stability and exhibit a reversal in sign of the lateral stability (slope of C_l plotted against β) at very low sideslip angles, the reversals being smaller for the N_1 nose shape. Essentially no effects of nose and body shape are noted for the configurations with fins off in figure 14.

Effects of vertical fins.- As seen in figure 14 at both $M = 9.6$ and $M = 17.8$, the configurations with vertical fins off have very smooth variations in directional and lateral aerodynamic characteristics. It is only when the vertical fins are placed on the vehicle that the reversal in roll characteristics mentioned previously is noted. This

nonlinearity increases as the fin area is increased (compare configurations with V_1 and V_3 fins) and is most severe for the blunt leading-edge fins, V_2. Figure 15, which presents the effects of each of the V_1 vertical fins on the directional and lateral aerodynamic characteristics of the configuration, indicates that the nonlinear input is produced by the leeward fin (V_{1L}) and not the windward (V_{1R}). Figure 4(a) shows the body shock to lie very close to the vertical fins and to move outboard of the leeward fin as the sideslip angle is increased. This shock motion could produce an interaction on the leeward fin at low sideslip angles which subsides at higher angles and thus creates the slope reversals in rolling moment noted. In reference 8, a similar shock interaction on a cranked-wing vehicle was noted to have a strong effect on the directional characteristics of the vehicle.

Effects of vertical-fin rollout.- References 3 and 8 have shown that by rolling the fins out at hypersonic speeds, increases in directional stability can be realized at high angles of attack. The V_3 fins on configuration $W_1N_{2C}B_2$ were rolled out 20° from the vertical, and the results at $M = 9.6$ and $\alpha = 0°$ are presented in figure 16. At sideslip angles below about 5° the nonlinearity of the rolling- and yawing-moment curves are reduced by fin rollout, although the general levels of the moments are not changed. At higher sideslip angles, negative increments in both rolling and yawing moments result from the fin rollout, with the decrease in yawing moment being a result of the decreased projected sideview area of the fin as well as shock interaction effects (see fig. 4(b)). Schlieren photographs in figure 4(b) show that the body shock lies very close to the rolled out fins and may cause some interaction effects.

Effects of body flap.- Deflecting the body flap 60° to provide low-angle-of-attack longitudinal stability to configuration $W_1N_{2C}B_2V_1$ had little effect on the directional and lateral characteristics of the vehicle at $\alpha = 0°$ as seen in figure 17. At the higher sideslip angles a negative increment in rolling moment is produced by the side force on the flap acting well above the vehicle center of gravity. A positive increment in yawing moment is likewise produced since the side force on the flap acts well behind the vehicle center of gravity.

Directional and Lateral Aerodynamic Characteristics at an Angle of Attack of 10°

The effects of nose shape and vertical fins on the directional and lateral aerodynamic characteristics of the vehicles are presented at

$M = 9.6$ in figures 18 and 19 at an angle of attack of 10°. It is interesting to note that the slope reversals in rolling moment and yawing moment which were quite evident at $\alpha = 0^\circ$ have disappeared at $\alpha = 10^\circ$ for all configurations except configuration $W_1N_{2C}B_2V_2$. These blunt leading-edge fins, V_2, still produce large nonlinearities in yawing moment at the higher angle of attack, and this characteristic would probably be a serious drawback to their use in improving low-angle-of-attack longitudinal stability.

CONCLUDING REMARKS

An investigation has been carried out in the Langley 11-inch hypersonic tunnel to study the effects of several nose, vertical fin, and body-flap modifications on the low-angle-of-attack static stability characteristics of a winged reentry vehicle. From an analysis of the data, it is noted that configurations with slender bodies which are inboard of the wing leading edge in the apex region generally have longitudinal stability at low and zero angles of attack. However, configurations with bodies which extend to the wing leading edge near the nose generally have longitudinal instability in the same angle-of-attack range. Modification of the noses to include various canopy shapes had little effect on the stability.

Adding very blunt leading edges to the vertical fins reduced the angle-of-attack range over which the configuration was unstable, but increased the nonlinear moment characteristics about all three axes.

The use of a body flap located rearward on the upper surface of the vehicle proved to be the most successful method of providing longitudinal stability for the more blunt-nose configuration at low angles of attack. By use of the flap, the vehicle was stable at all angles of attack tested with little or no effect on either performance characteristics or lateral and directional stability.

A body shock interaction on the vertical fins created slope reversals in the lateral characteristics at low sideslip angles and at an angle of attack of 0°. At an angle of attack of 10°, these slope reversals were essentially nonexistent.

Langley Research Center,
National Aeronautics and Space Administration,
Langley Air Force Base, Va., August 24, 1961.

REFERENCES

1. Ladson, Charles L., and Johnston, Patrick J.: Aerodynamic Characteristics of Two Winged Reentry Vehicles at Supersonic and Hypersonic Speeds. NASA TM X-346, 1961.

2. Ladson, Charles L., and Johnston, Patrick J.: Aerodynamic Characteristics of a Blunt-Nosed Winged Reentry Vehicle at Supersonic and Hypersonic Speeds. NASA TM X-357, 1961.

3. Rainey, Robert W., and Close, William H.: Studies of Stability and Control of Winged Reentry Configurations. NASA TM X-327, 1960.

4. Bertram, Mitchel H.: Boundary-Layer Displacement Effects in Air at Mach Numbers of 6.8 and 9.6. NASA TR R-22, 1959. (Supersedes NACA TN 4133.)

5. Armstrong, William O., and Ladson, Charles L. (with Appendix A by Donald L. Baradell and Thomas A. Blackstock): Effects of Variation in Body Orientation and Wing and Body Geometry on Lift-Drag Characteristics of a Series of Wing-Body Combinations at Mach Numbers From 3 to 18. NASA TM X-73, 1959.

6. Henderson, Arthur, Jr., and Baradell, Donald L.: Recent Work at Langley Research Center in the Development of Hypersonic Helium Tunnels. Proc. Nat. Symposium on Hypervelocity Techniques (Denver, Colo.), Inst. Aero. Sci., Oct. 20-21, 1960, pp. 131-141.

7. Ladson, Charles L., Johnston, Patrick J., and Trescot, Charles D., Jr.: Effects of Wing Plan-Form Geometry on the Aerodynamic Characteristics of a Hypersonic Glider at Mach Numbers up to 9.6. NASA TM X-286, 1960.

8. Ladson, Charles L.: Directional and Lateral Stability Characteristics of a Winged Reentry Vehicle at Hypersonic Speeds. NASA TM X-550, 1961.

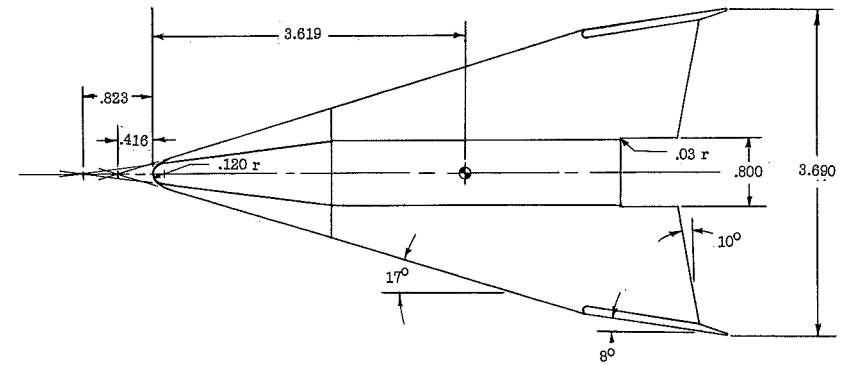

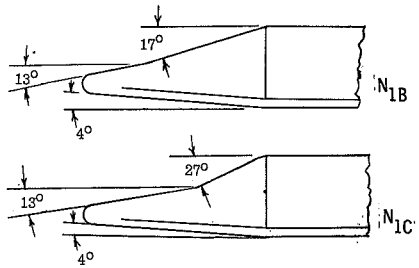

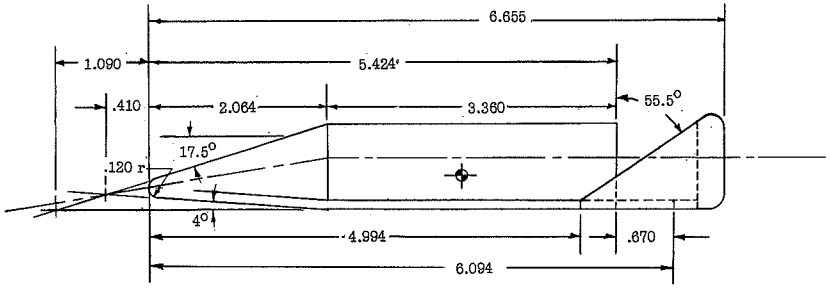

$W_1N_{1A}B_1V_1$

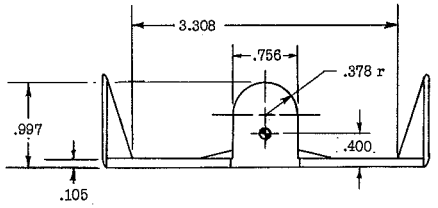

(a) Configuration $W_1N_{1A}B_1V_1$ and noses N_{1B} and N_{1C}.

Figure 1.- Drawings of models and model components.

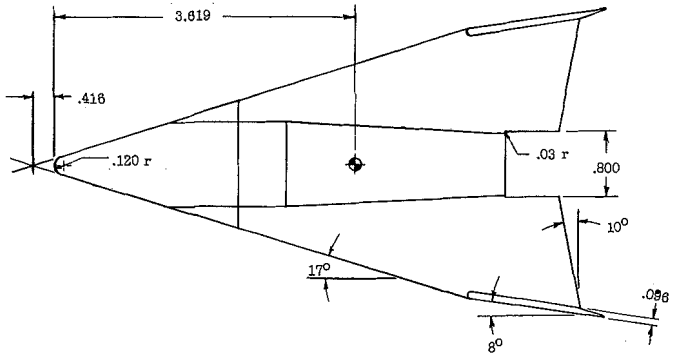

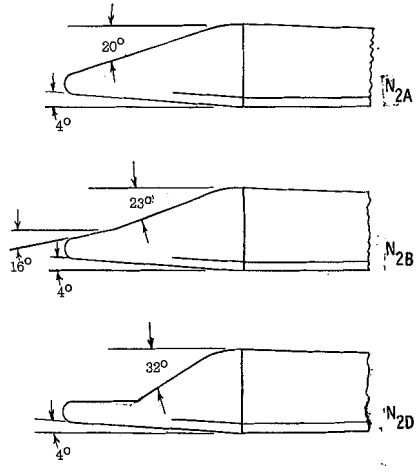

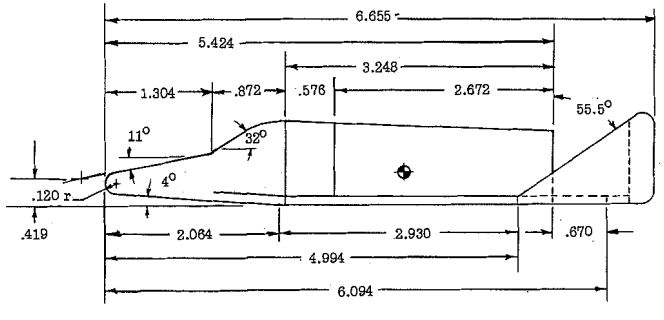

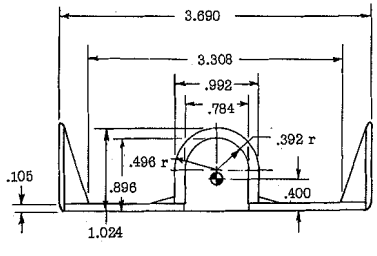

$W_1N_{2C}B_2V_1$

(b) Configuration $W_1N_{2C}B_2V_1$ and noses N_{2A}, N_{2B}, and N_{2D}.

Figure 1.- Continued.

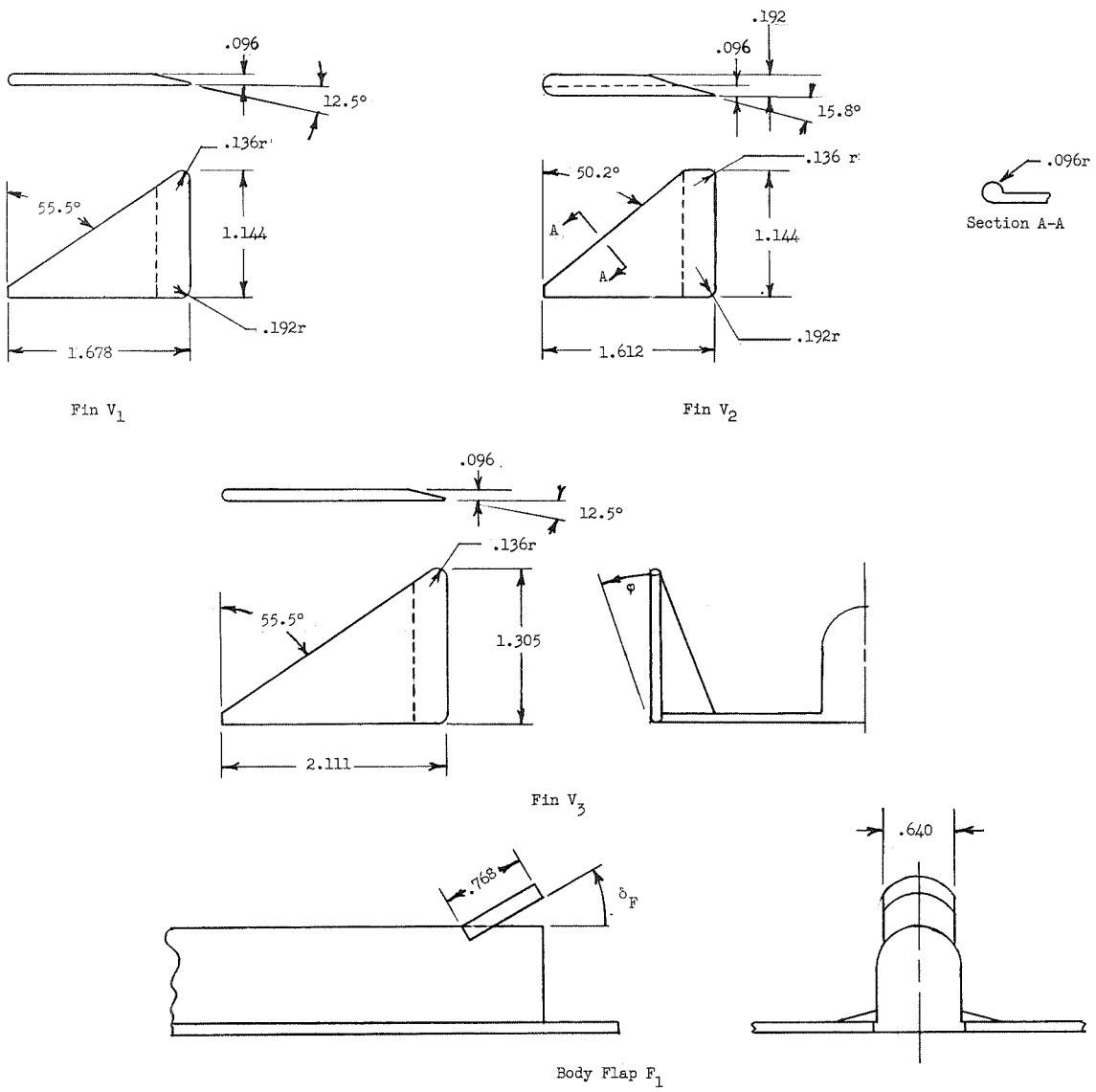

(c) Vertical fins V_1, V_2, and V_3; body flap F_1.

Figure 1.- Concluded.

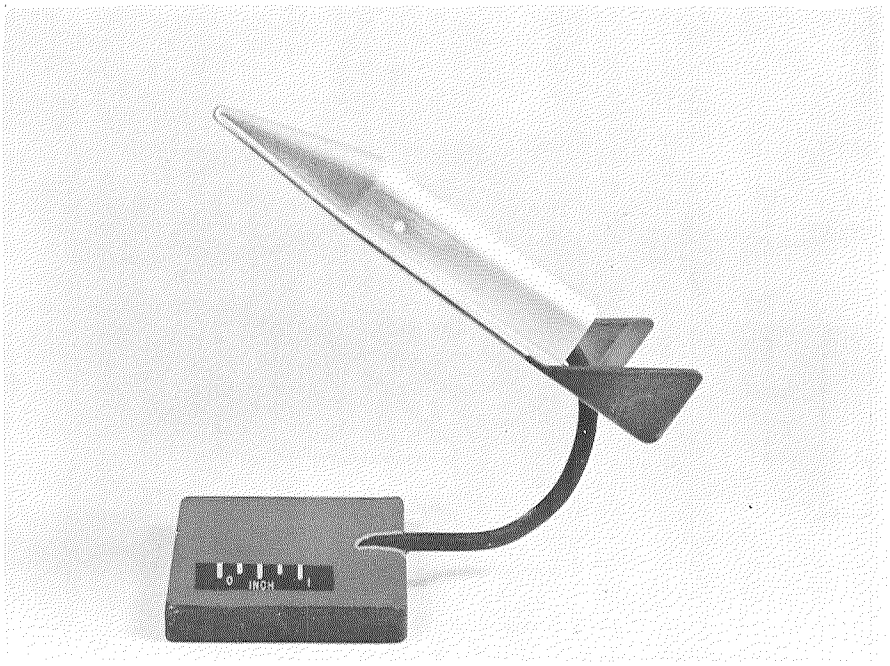

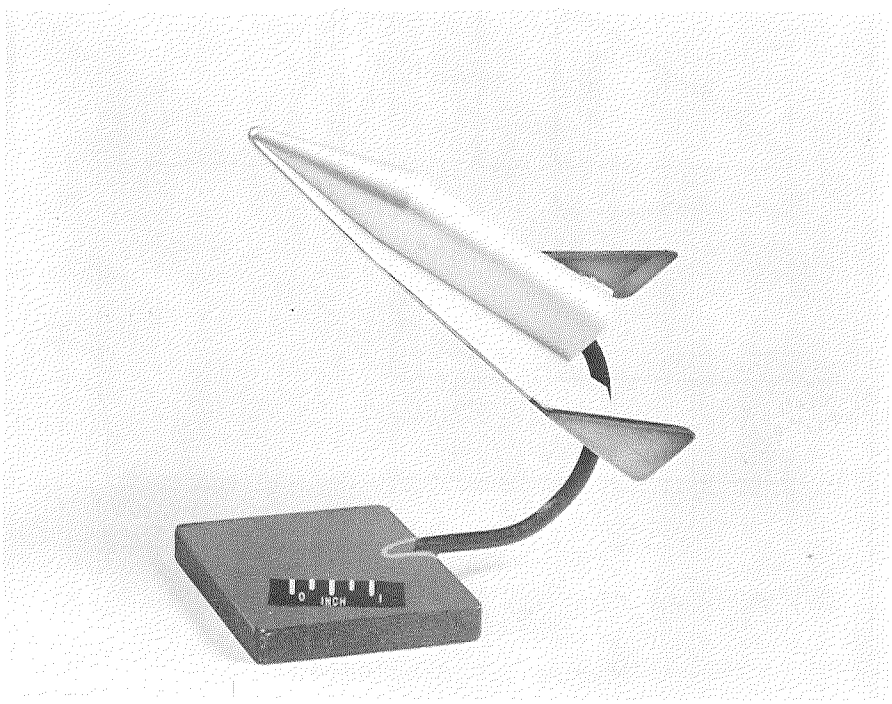

(a) Configuration $W_1N_1AB_1V_1$. L-61-5080

Figure 2.- Model photographs.

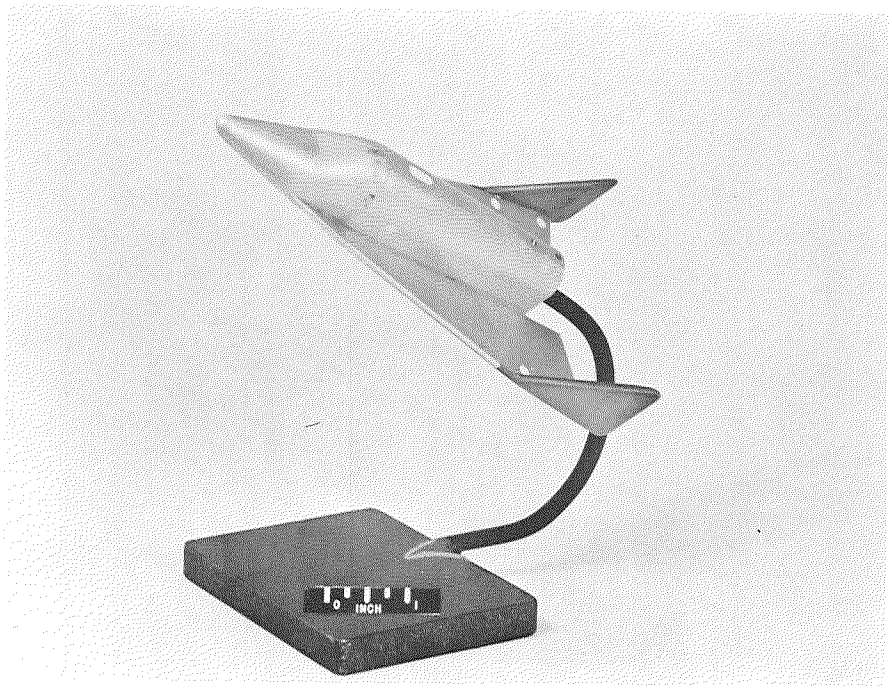

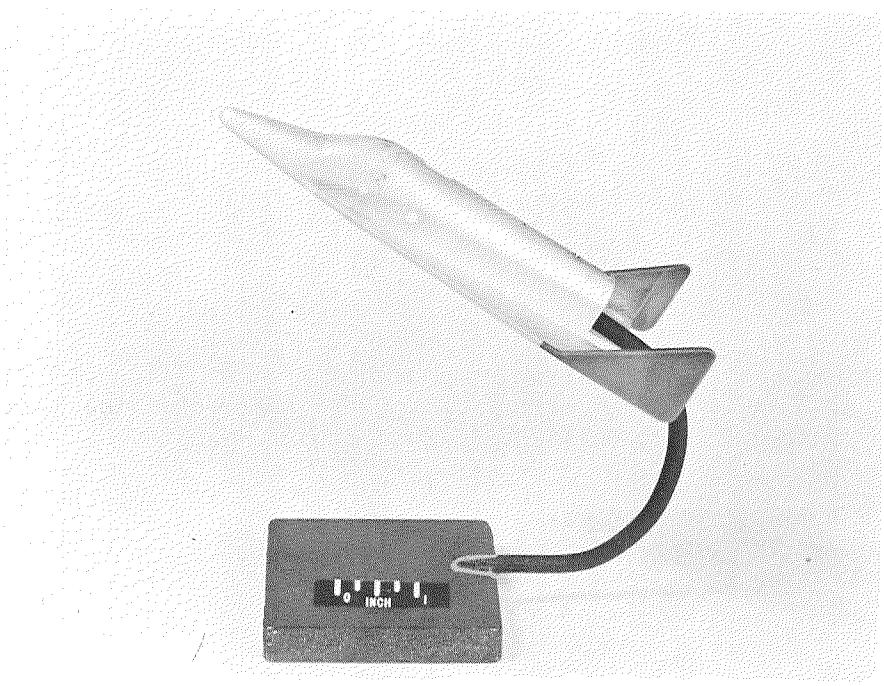

(b) Configuration $W_1N_{2C}B_2V_1$. L-61-5081

Figure 2.- Continued.

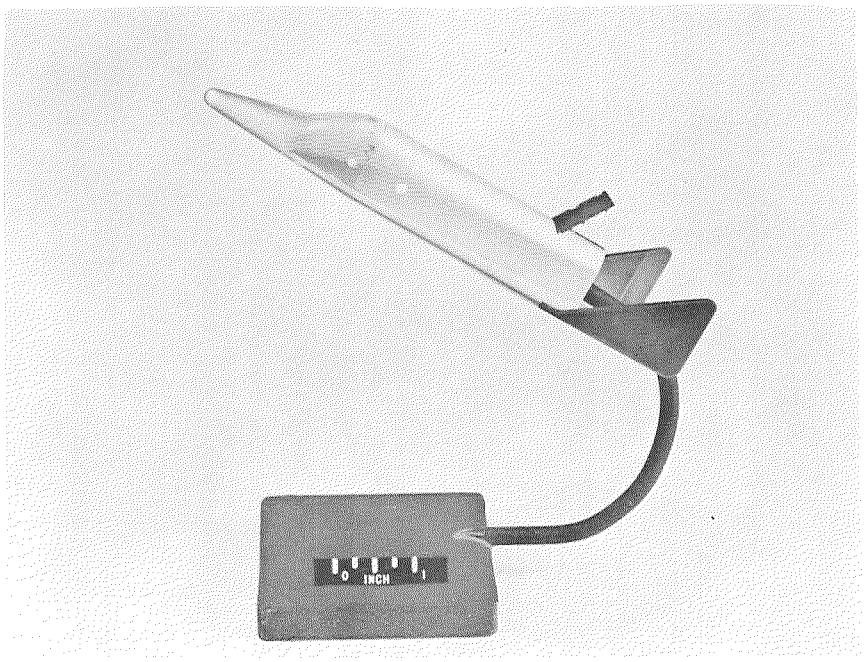

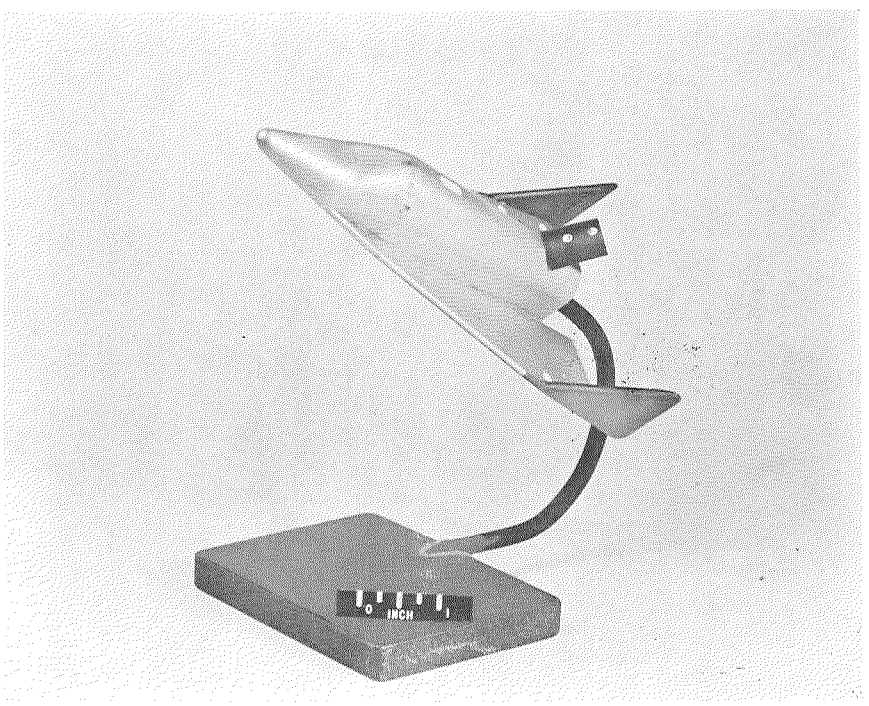

(c) Configuration $W_1N_{2C}B_2V_1F_1$; $\delta_F = 60^\circ$. L-61-5082

Figure 2.- Concluded.

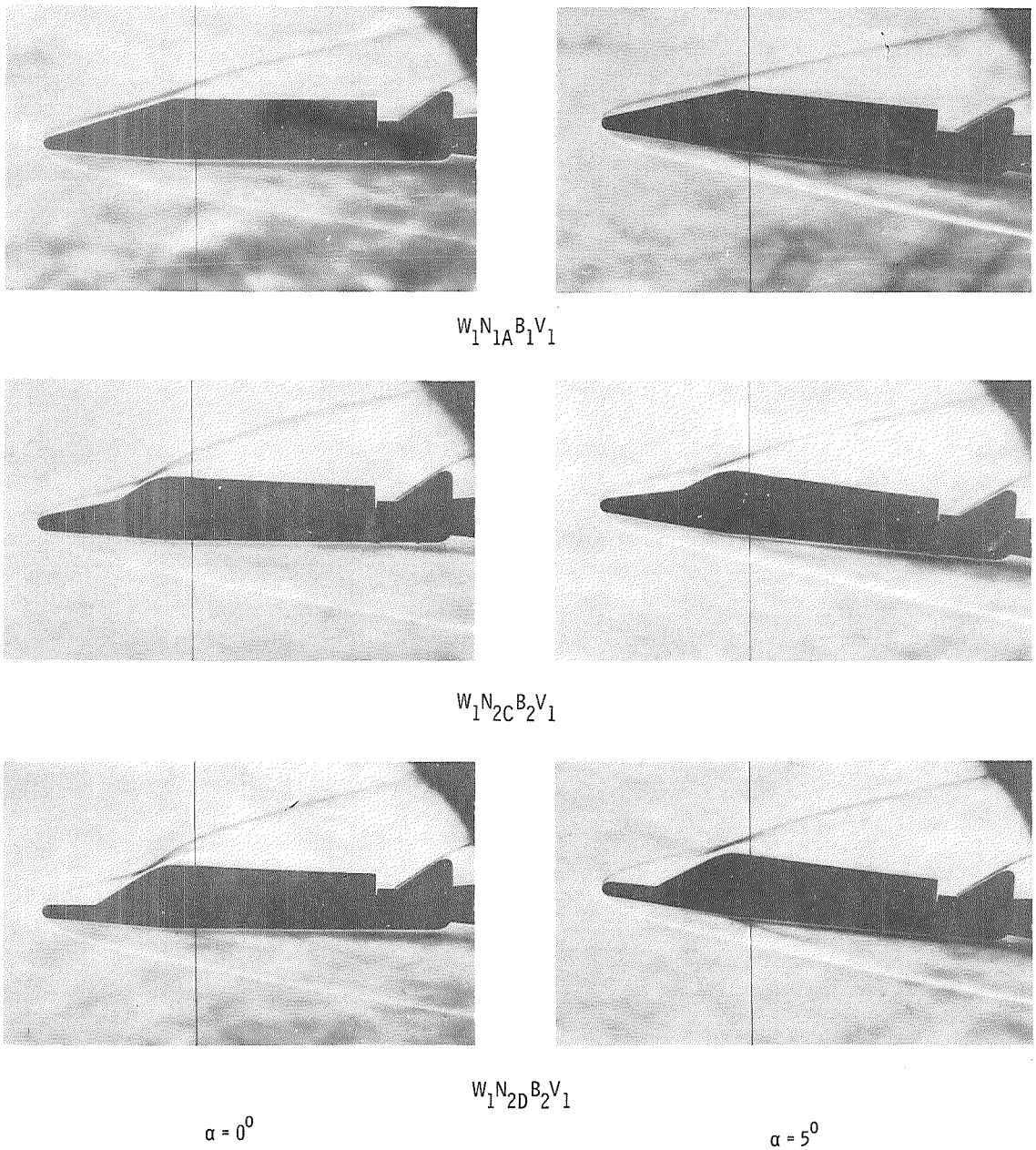

L-61-5075

Figure 3.- Effects of nose shape on shock pattern at M = 9.6.

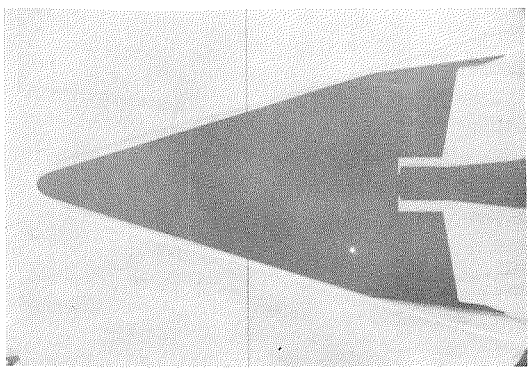

$\beta = 0^{o}$

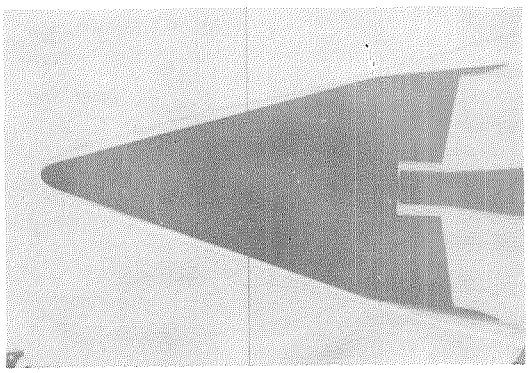

$\beta = 2^{o}$

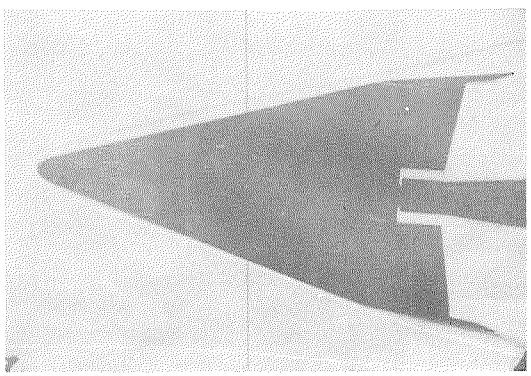

$\beta = 4^{o}$

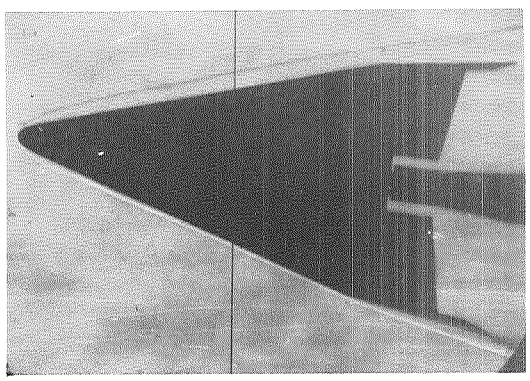

$\beta = 6^{o}$

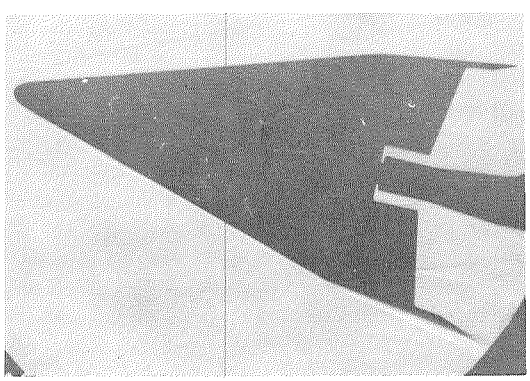

$\beta = 12^{o}$

(a) $\varphi = 0^{o}$. L-61-5076

Figure 4.- Effects of sideslip and fin rollout on shock pattern at M = 9.6. Configuration $W_1N_{2C}B_2V_3$.

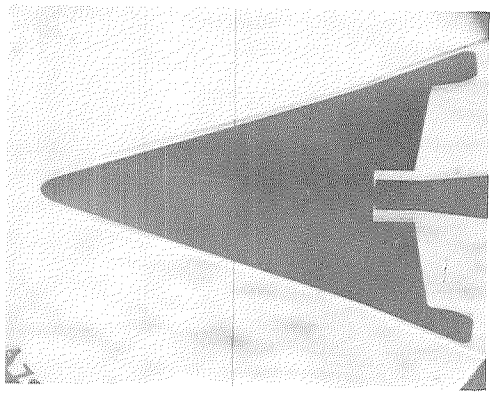

$\beta = 0^{\circ}$

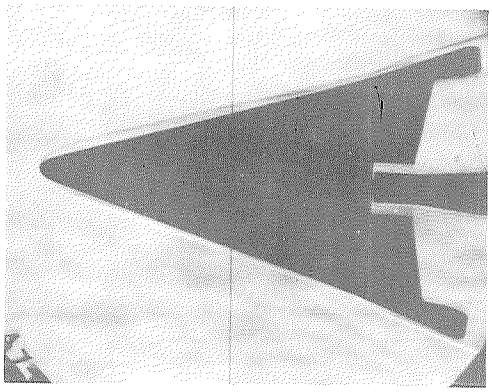

$\beta = 2^{\circ}$

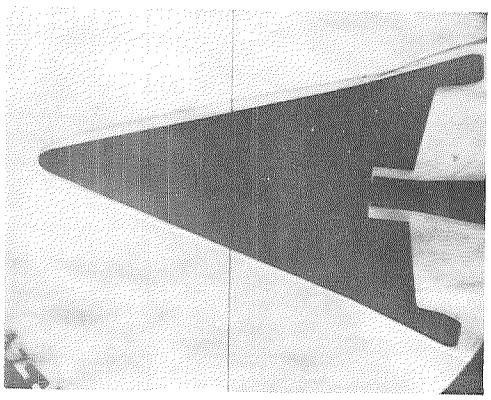

$\beta = 4^{\circ}$

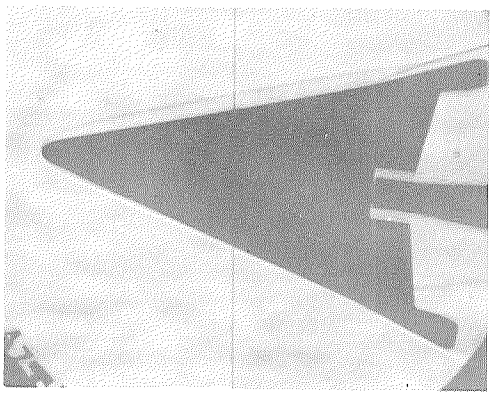

$\beta = 6^{\circ}$

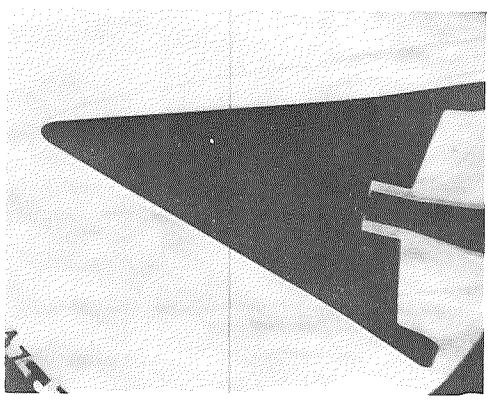

$\beta = 12^{\circ}$

(b) $\varphi = 20^{\circ}$.

L-61-5077

Figure 4.- Concluded.

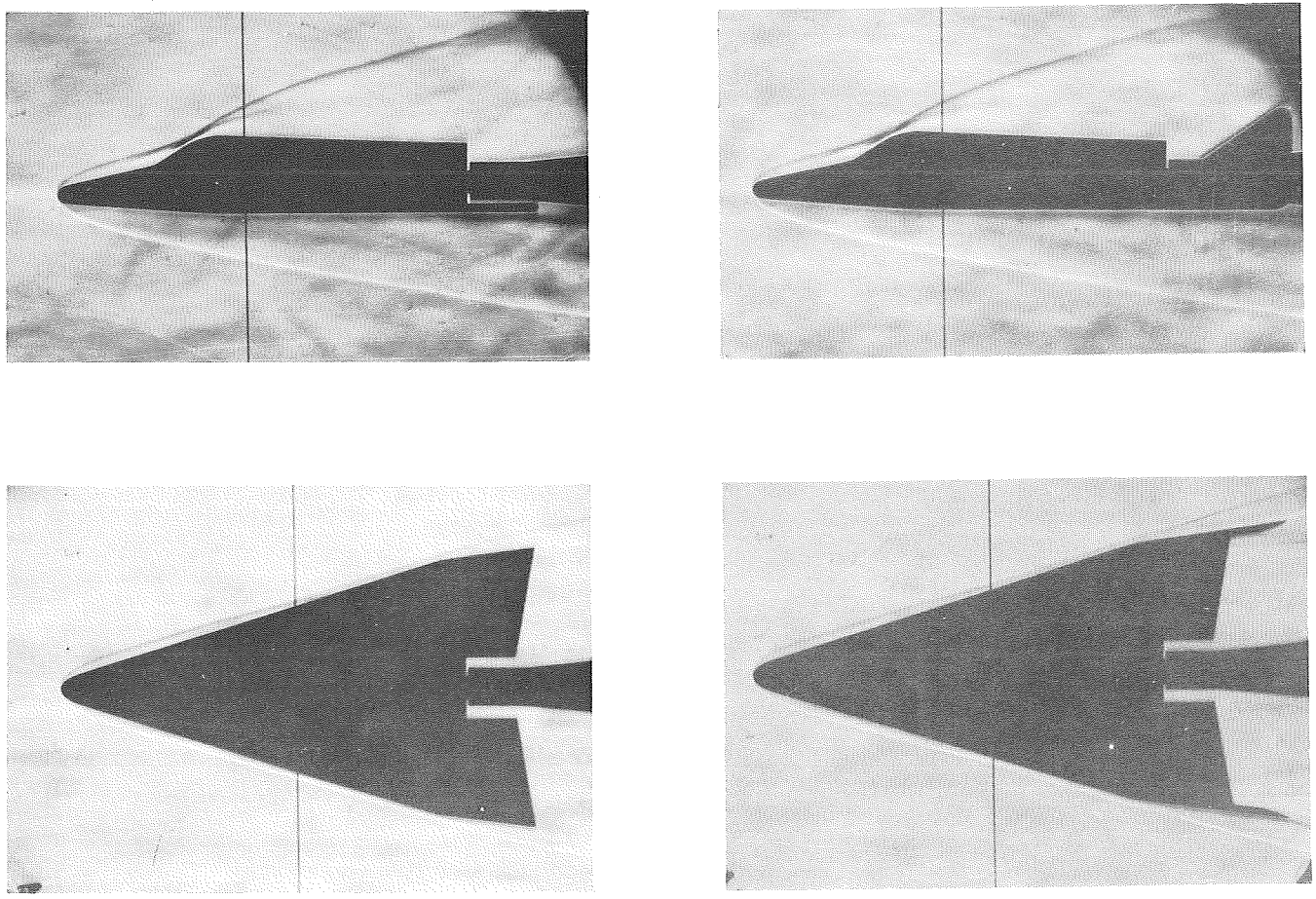

$W_1N_{2C}B_2V_0$ $W_1N_{2C}B_2V_3$

(a) M = 9.6 in air. L-61-5078

Figure 5.- Comparison of shock patterns at M = 9.6 in air and M = 17.8 in helium.

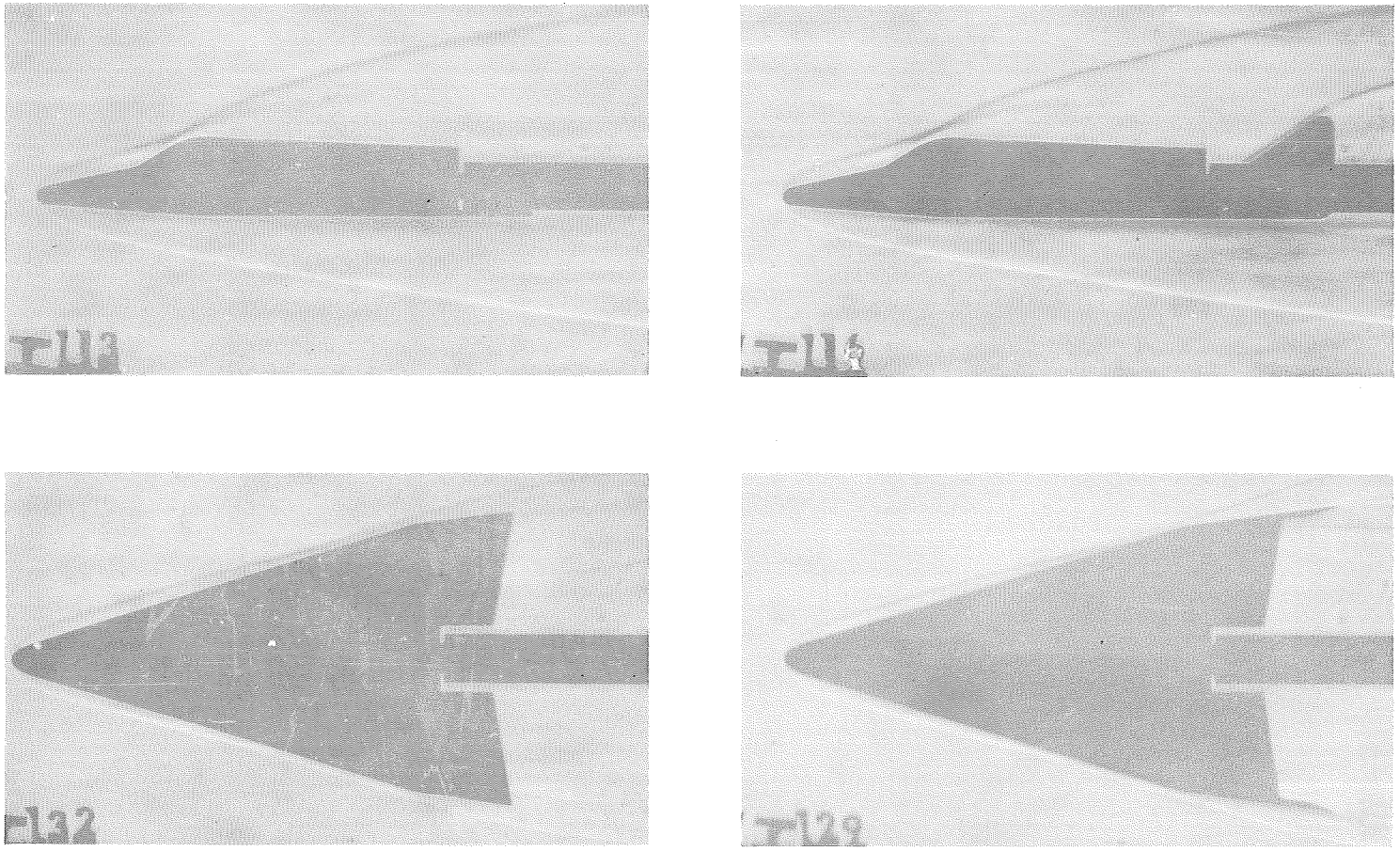

$W_1N_{2C}B_2V_0$ $W_1N_{2C}B_2V_3$

(b) M = 17.8 in helium. L-61-5079

Figure 5.- Concluded.

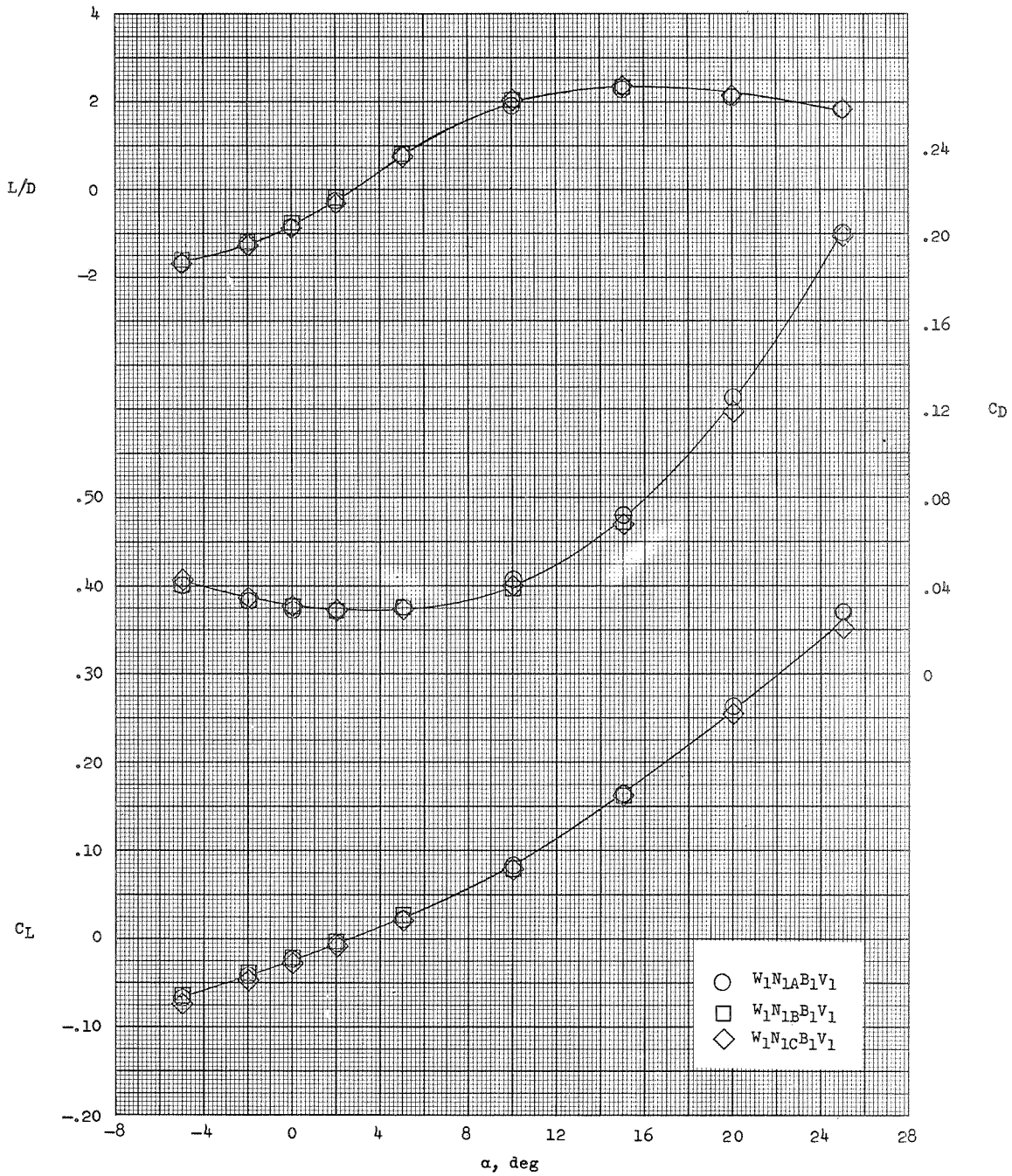

(a) Nose N_1.

Figure 6.- Effects of nose shape on longitudinal performance characteristics. M = 9.6.

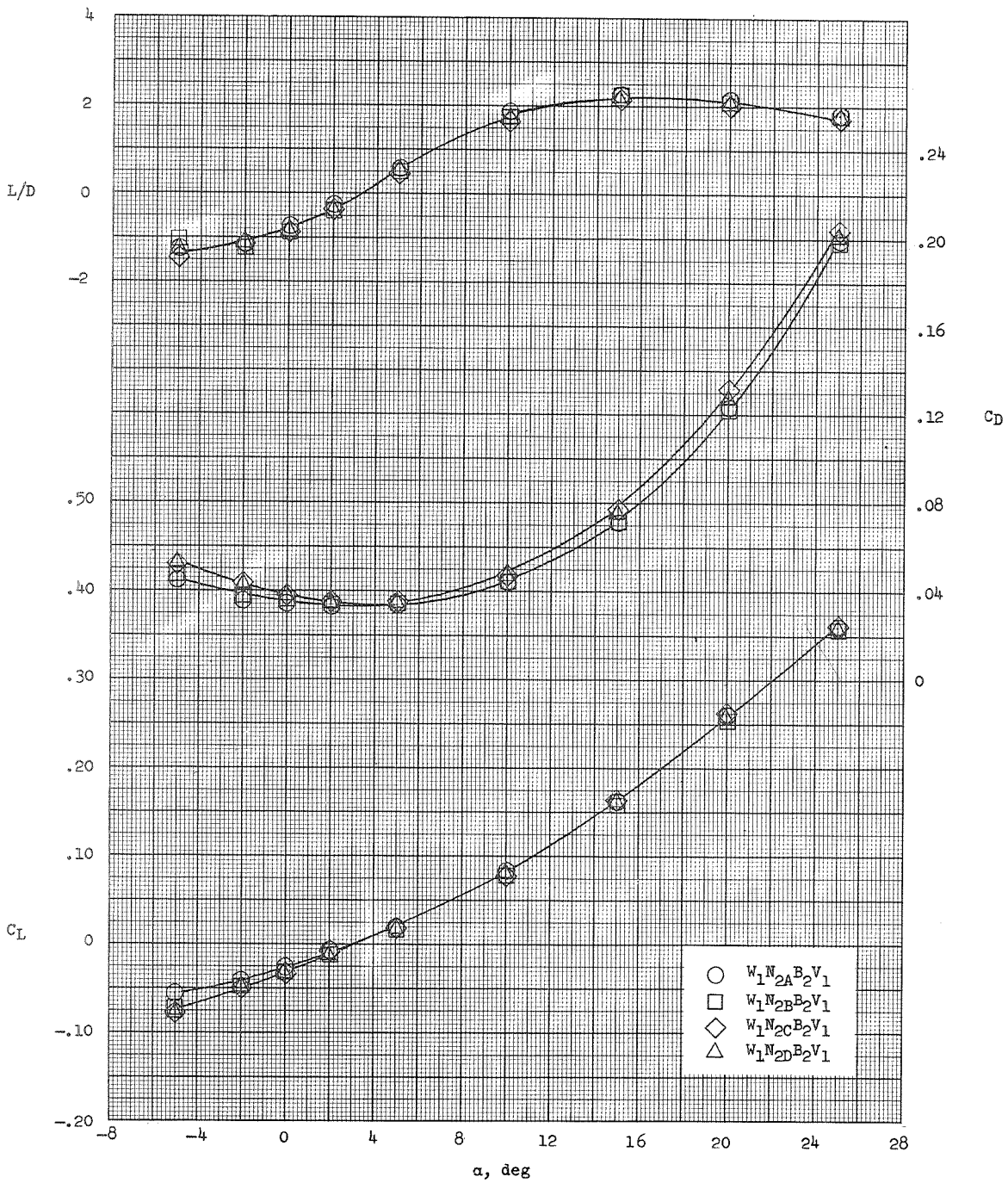

(b) Nose N_2.

Figure 6.- Concluded.

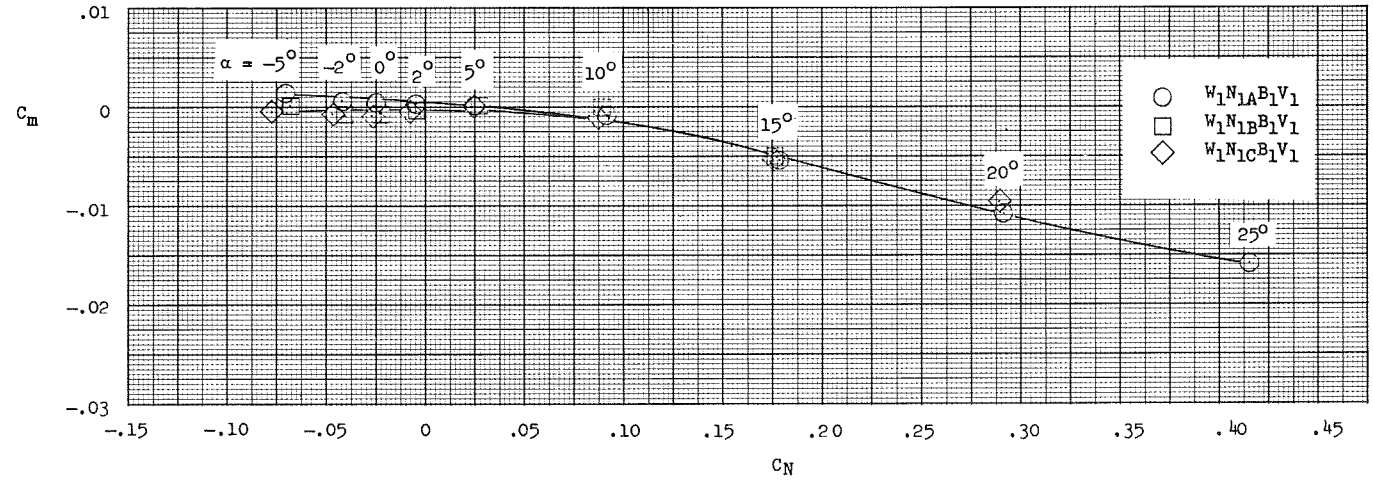

(a) Nose N_1.

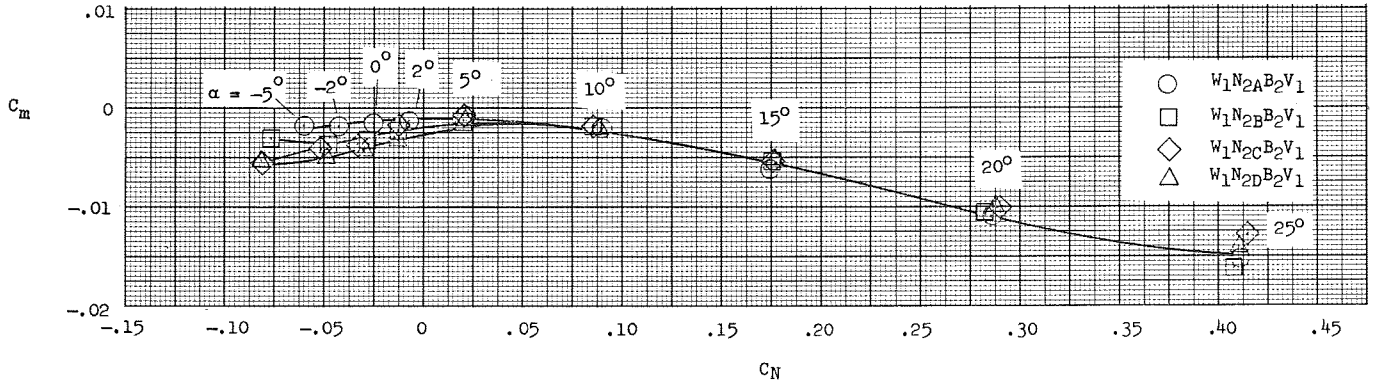

(b) Nose N_2.

Figure 7.- Effects of nose shape on longitudinal stability characteristics. M = 9.6.

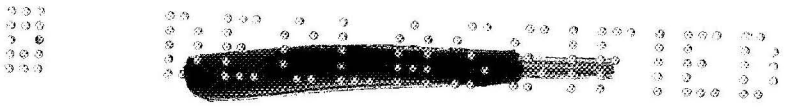

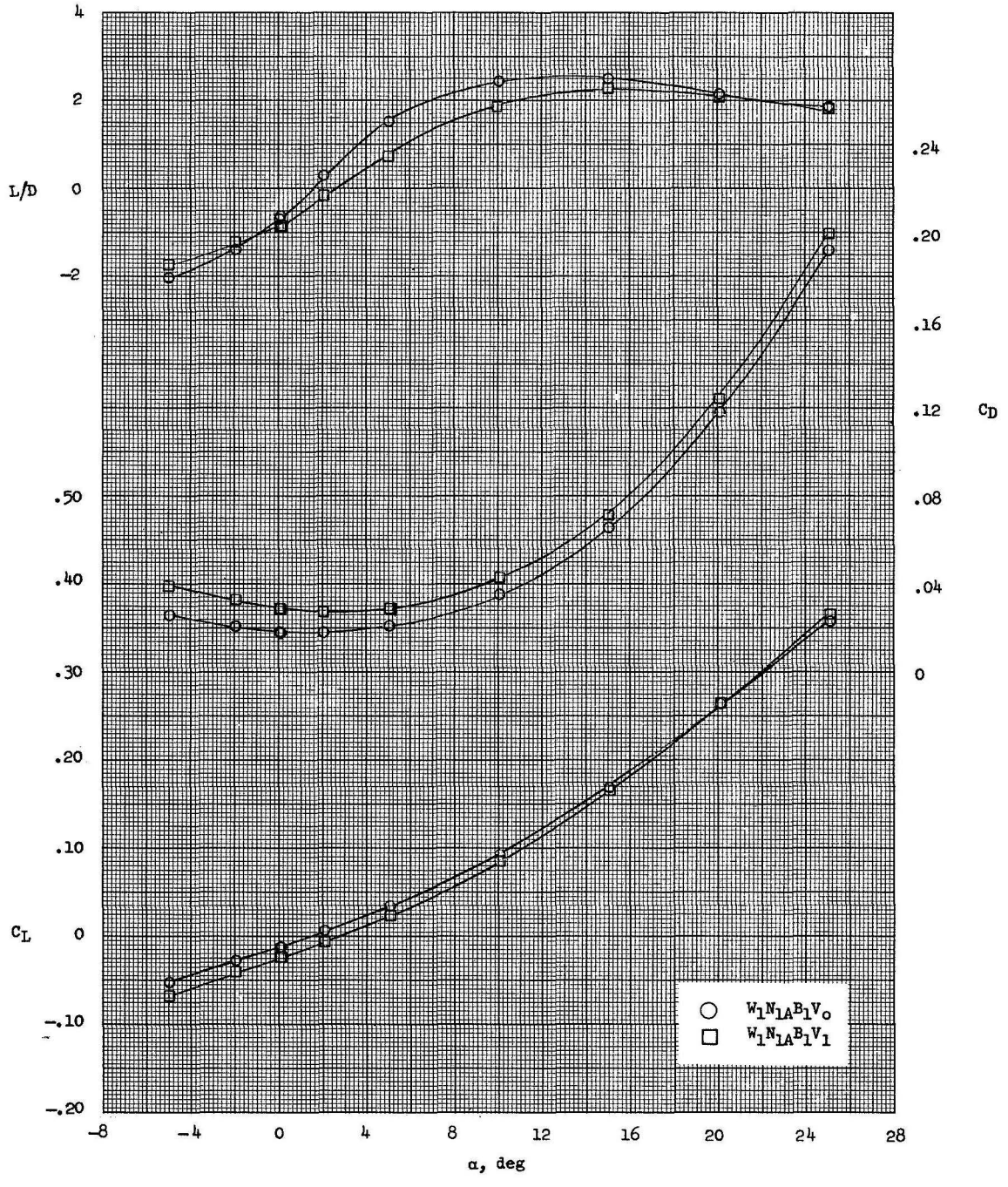

(a) Nose N_1; M = 9.6.

Figure 8.- Effect of vertical fin on longitudinal performance characteristics.

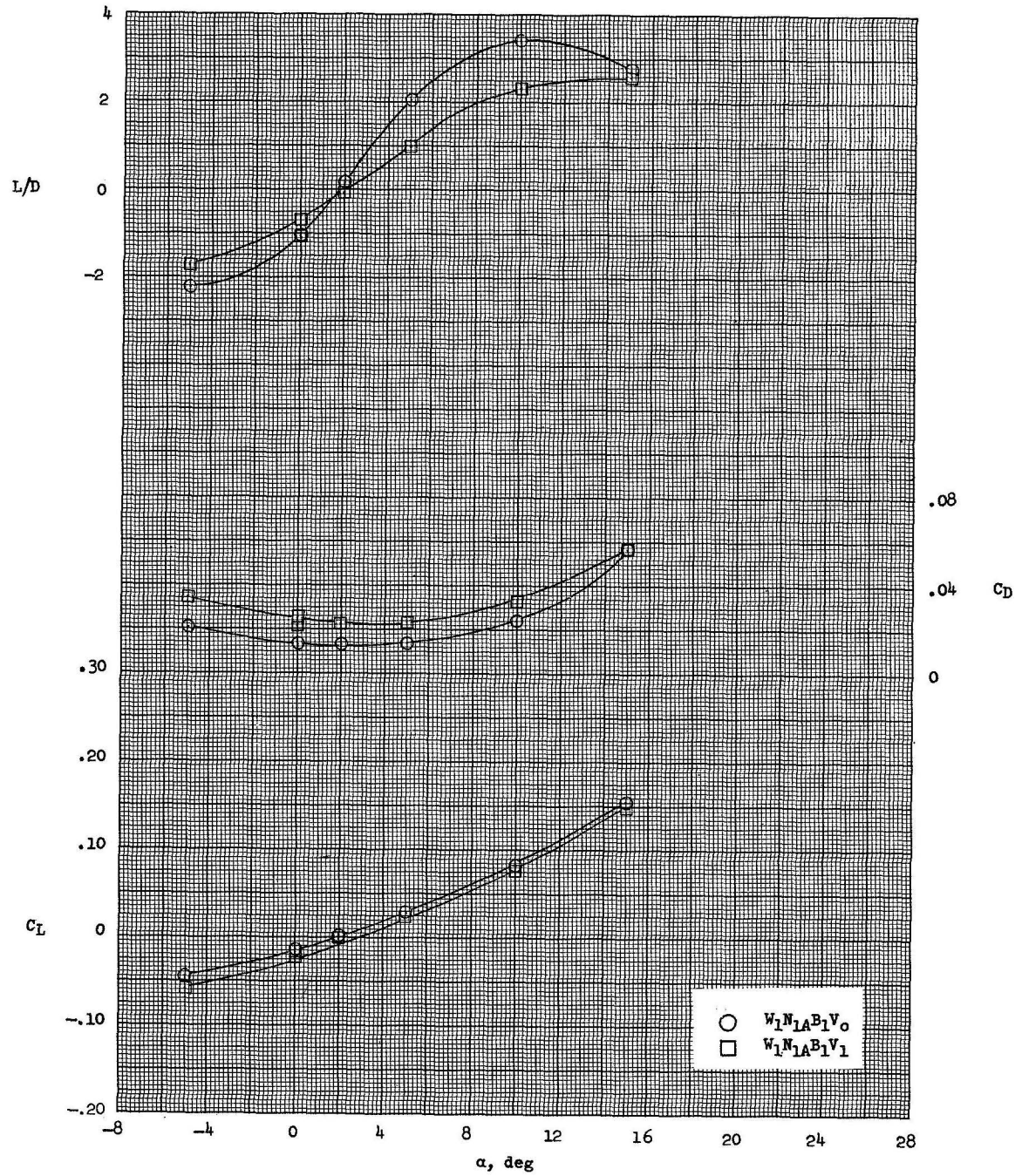

(b) Nose N_1; M = 17.8.

Figure 8.- Continued.

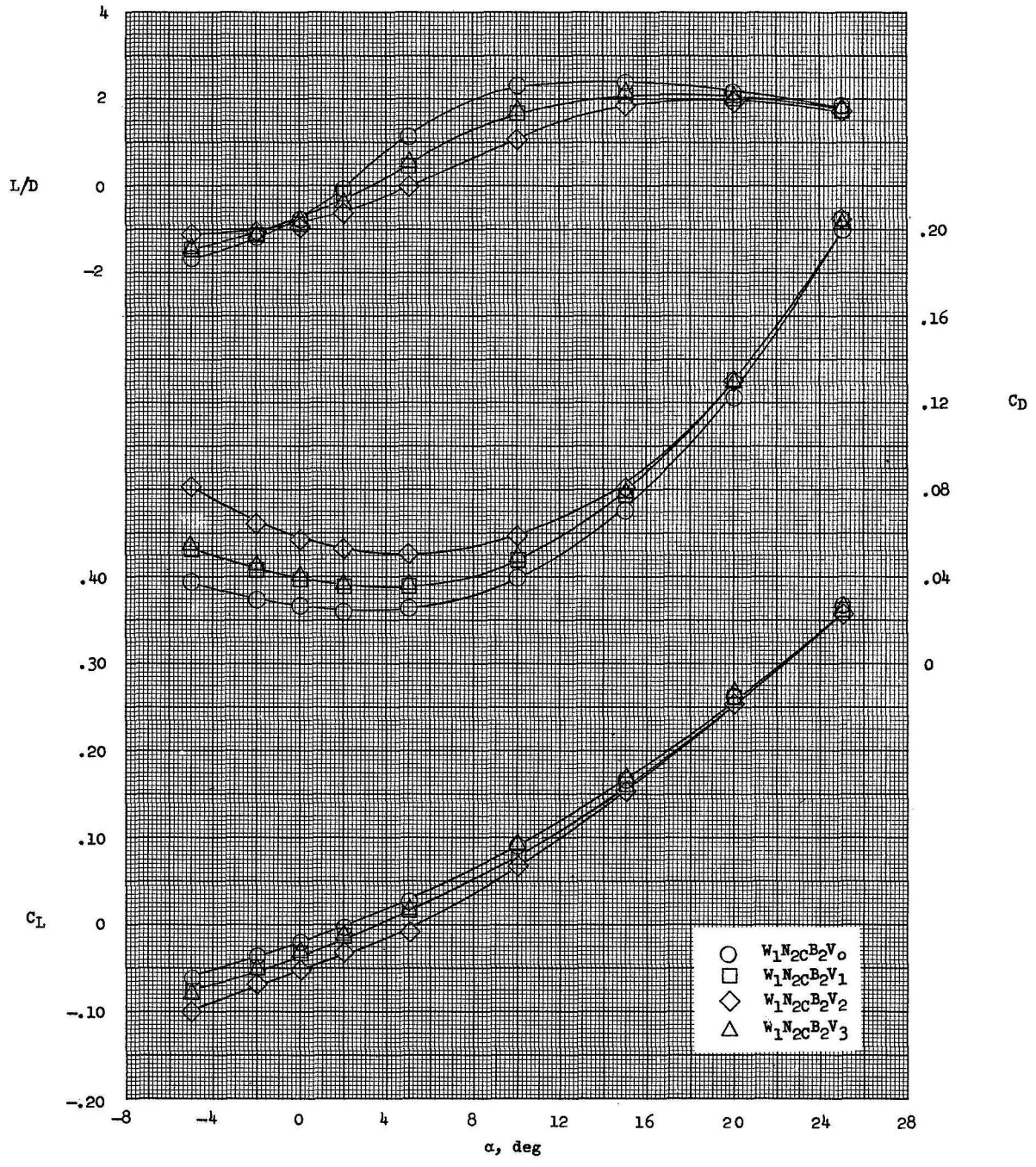

(c) Nose N_2; M = 9.6.

Figure 8.- Continued.

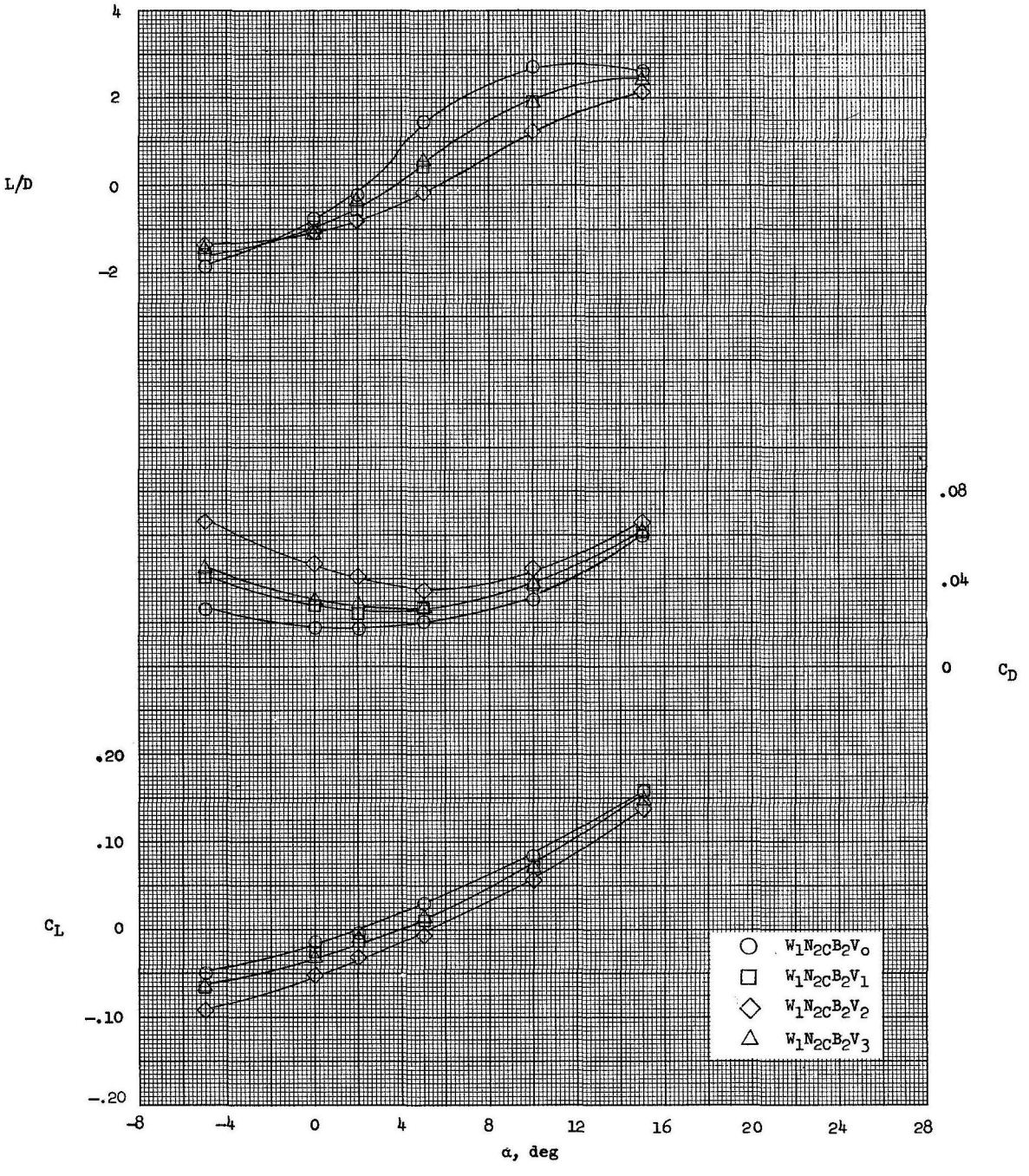

(d) Nose N_2; M = 17.8.

Figure 8.- Concluded.

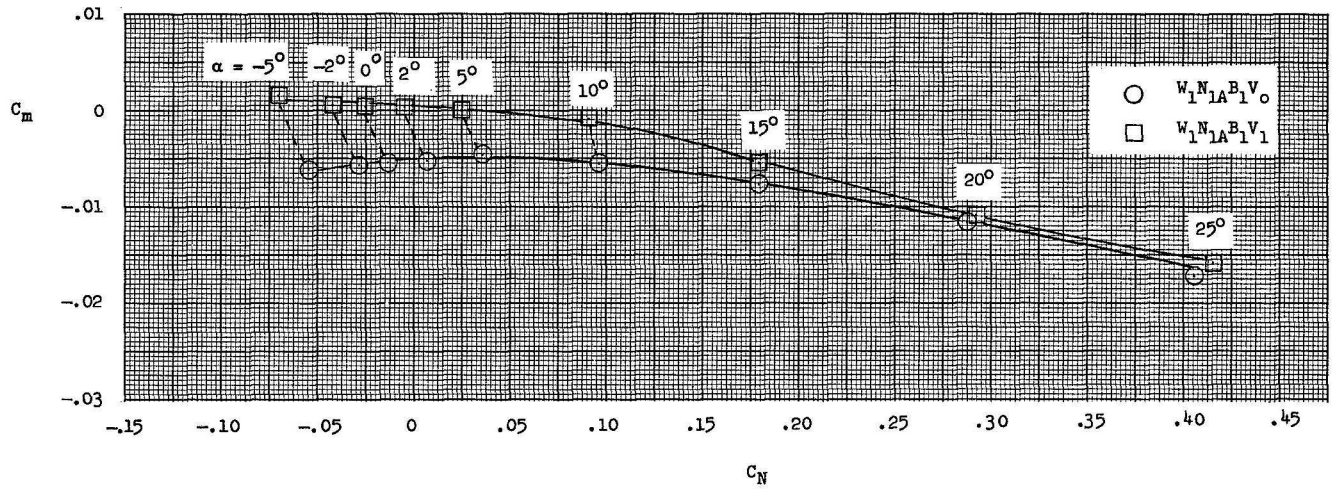

(a) Nose N_1; M = 9.6.

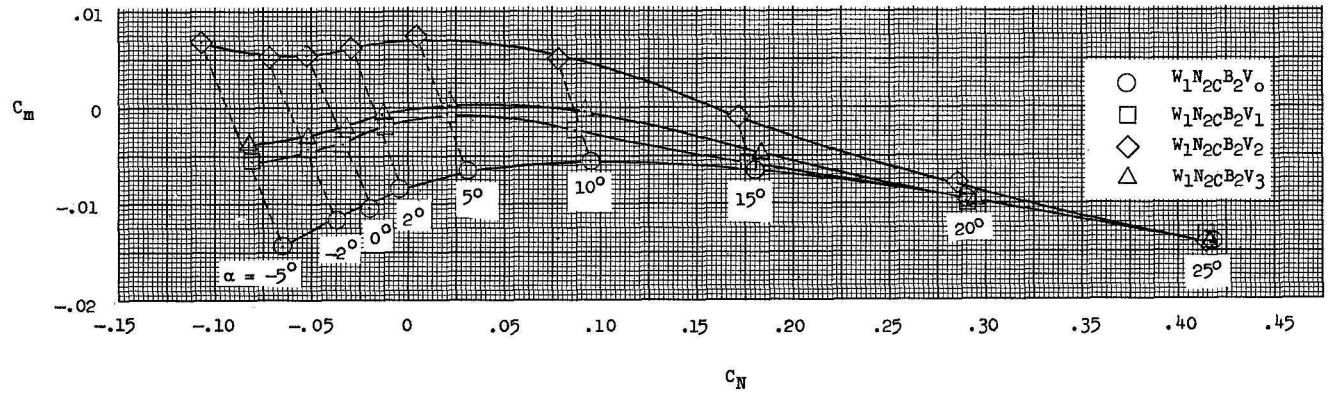

(b) Nose N_2; M = 9.6.

Figure 9.- Effects of vertical fins on longitudinal stability characteristics.

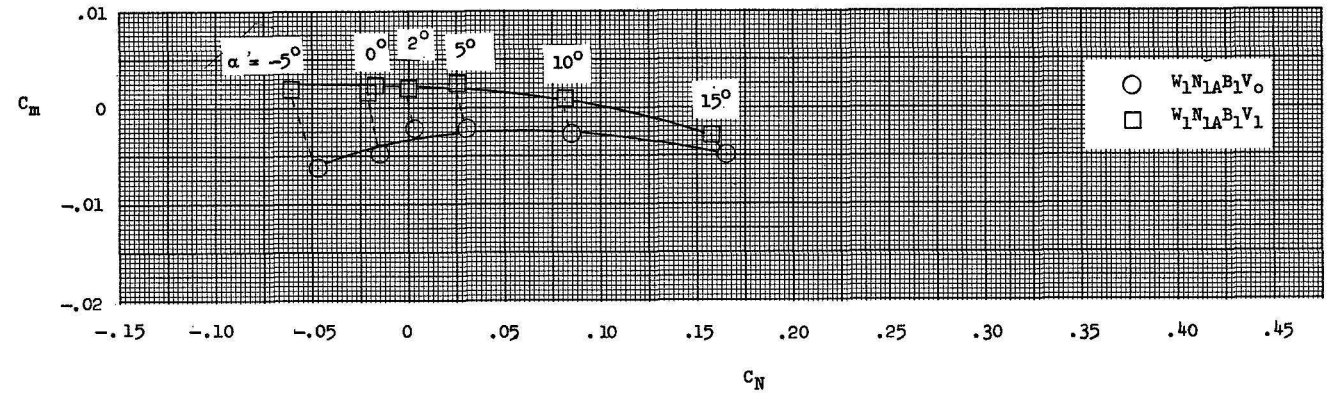

(c) Nose N_1; M = 17.8.

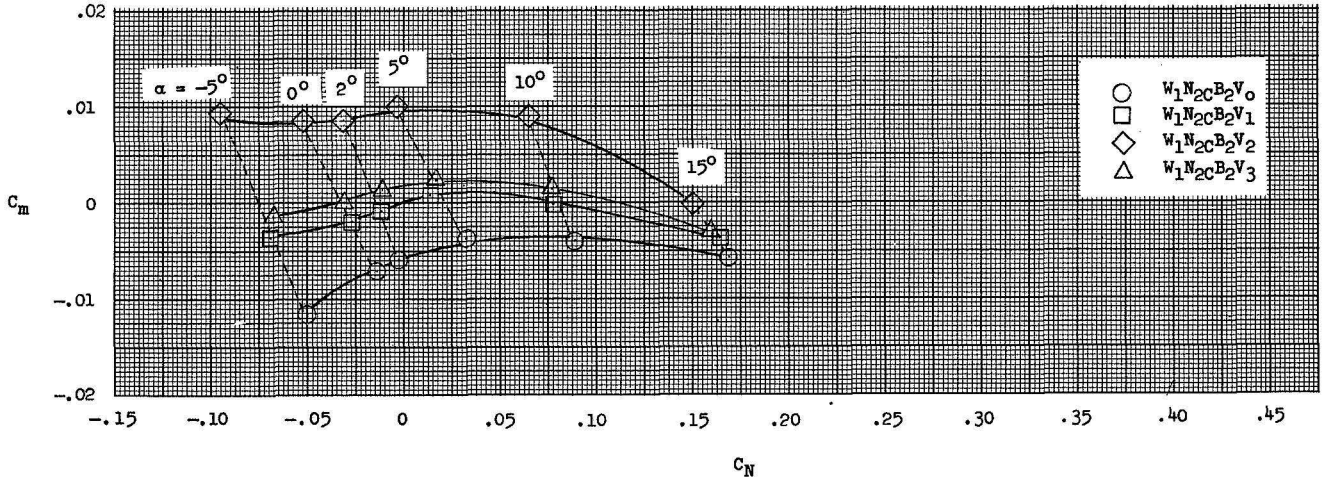

(d) Nose N_2; M = 17.8.

Figure 9.- Concluded.

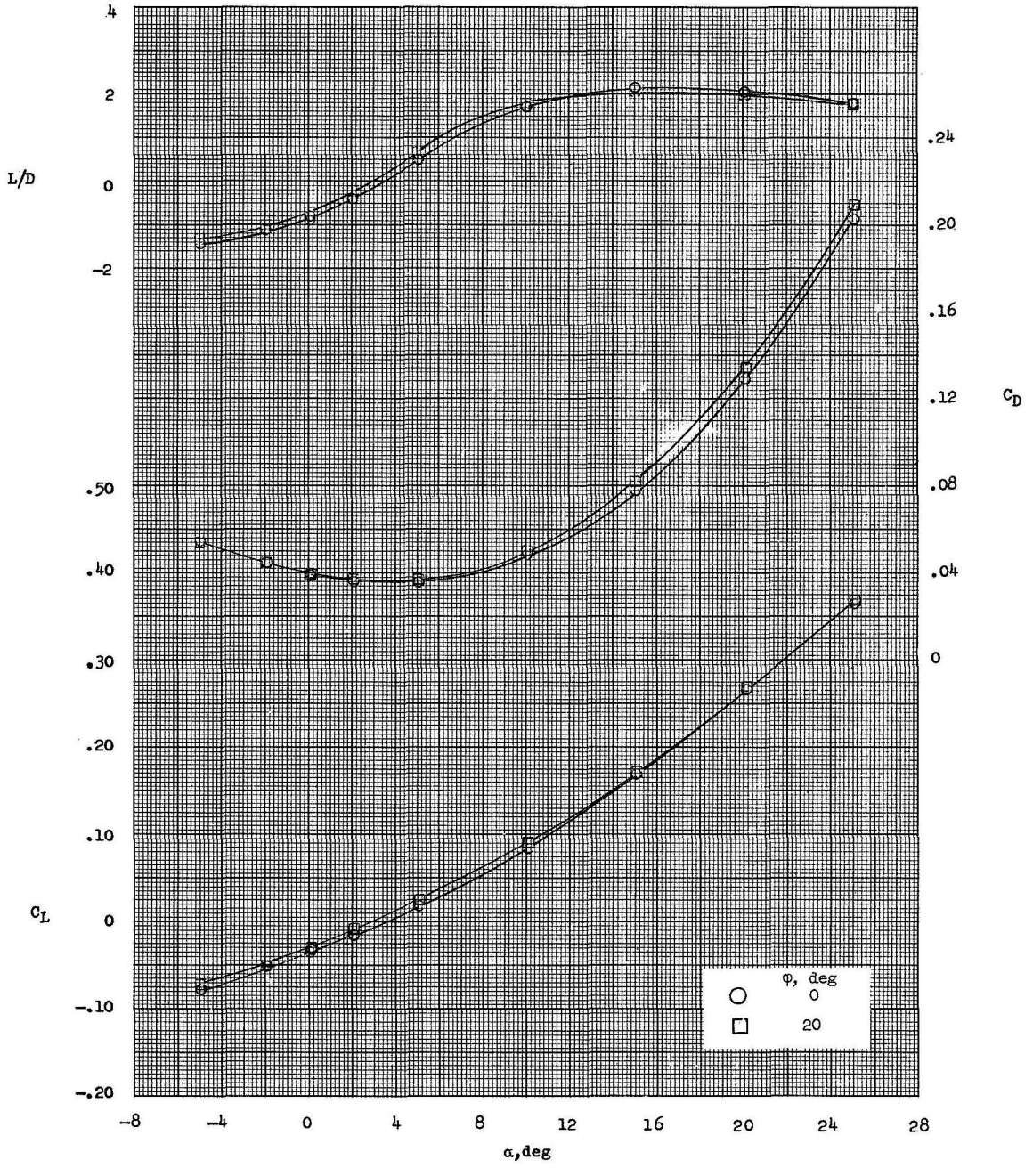

Figure 10.- Effect of vertical-fin rollout on longitudinal performance characteristics of configuration $W_1N_{2C}B_2V_3$. M = 9.6.

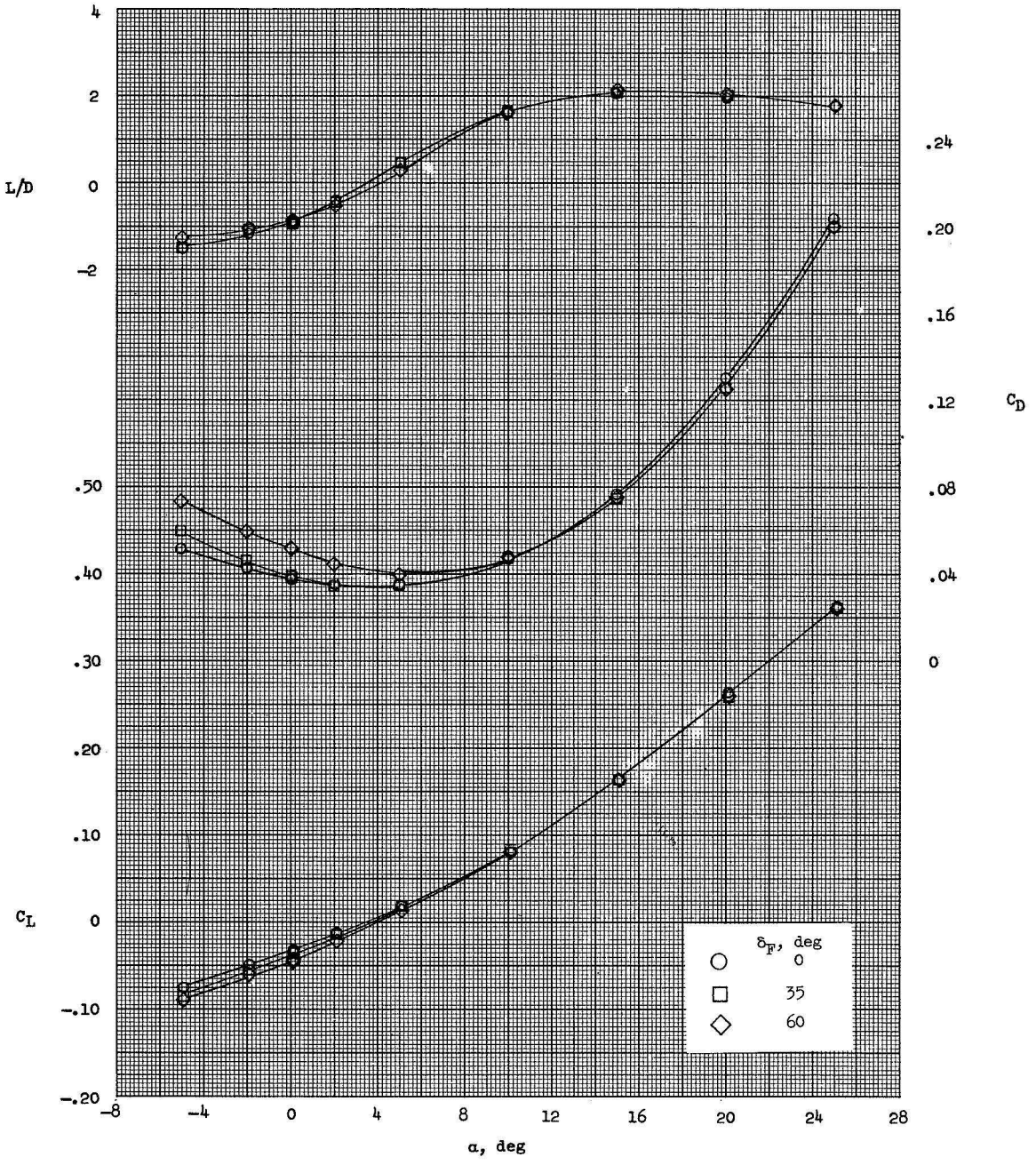

Figure 11.- Effect of body-flap deflection on longitudinal performance characteristics of configuration $W_1N_{2C}B_2V_1F_1$. M = 9.6.

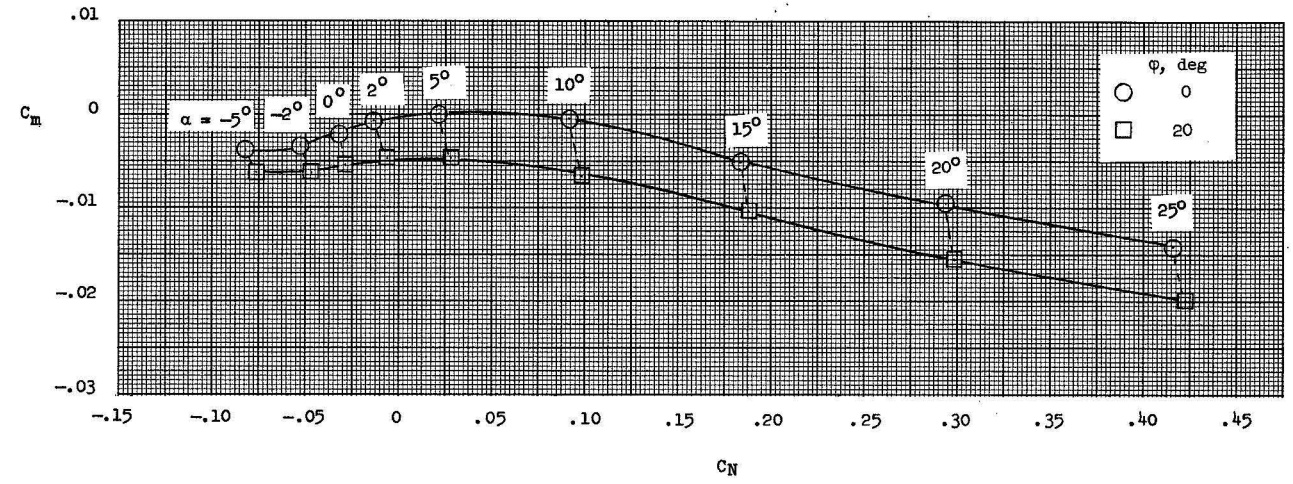

(a) Effects of fin rollout; configuration $W_1N_{2C}B_2V_3$.

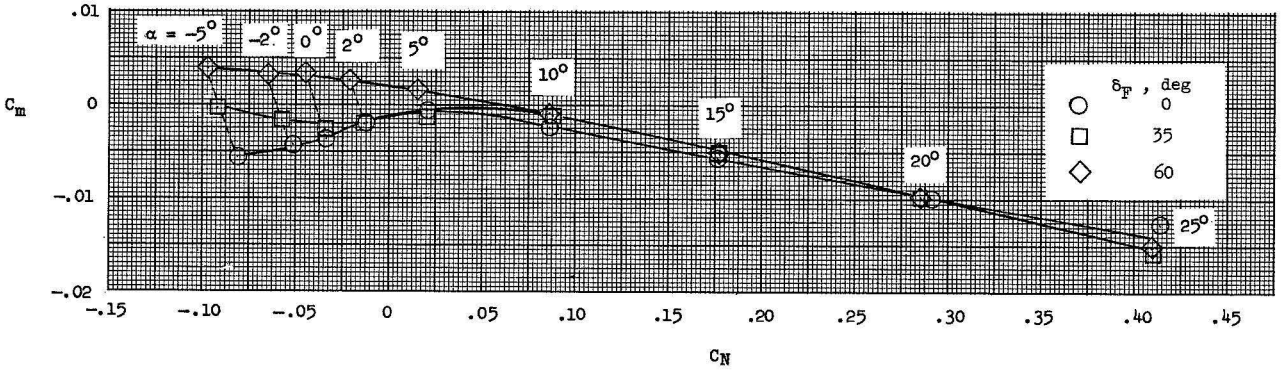

(b) Effects of body-flap deflection; configuration $W_1N_{2C}B_2V_1$.

Figure 12.- Effects of body-flap deflection and vertical-fin rollout on longitudinal stability characteristics. M = 9.6.

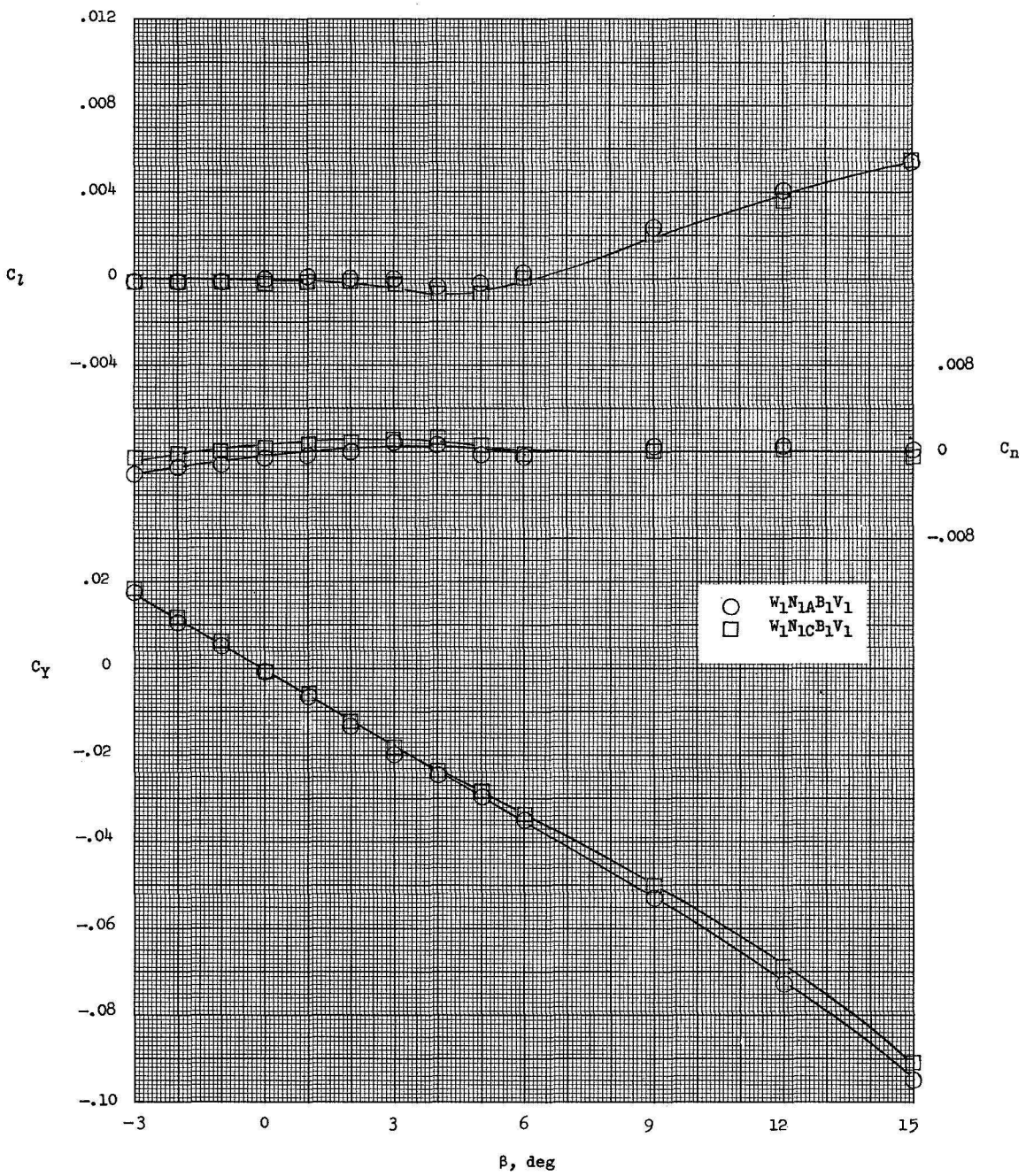

(a) Nose N_1.

Figure 13.- Effects of nose shape on directional and lateral aerodynamic characteristics at $\alpha = 0^{\circ}$. M = 9.6.

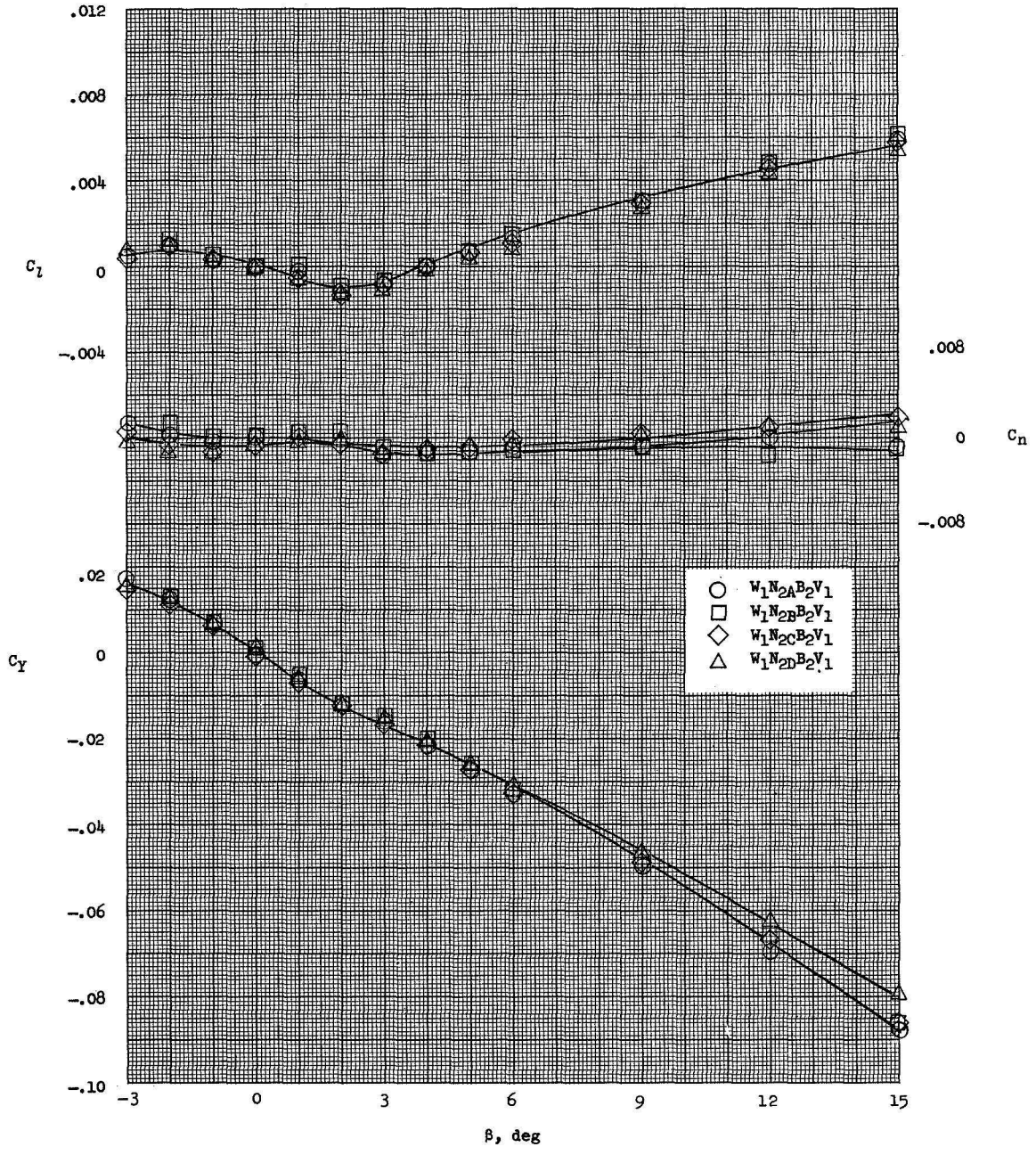

(b) Nose N_2.

Figure 13.- Concluded.

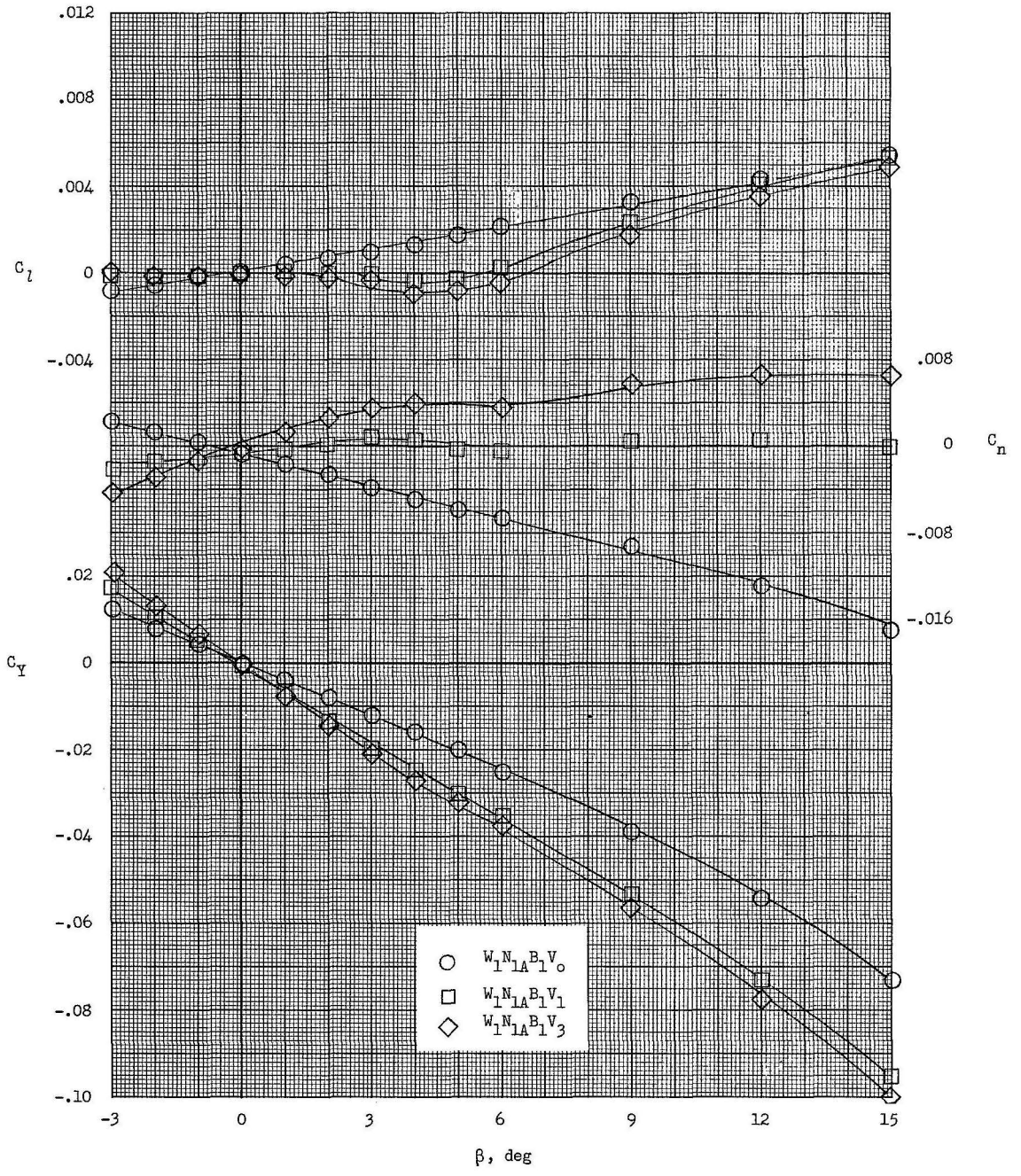

(a) Nose N_1; M = 9.6.

Figure 14.- Effect of vertical fins on directional and lateral aerodynamic characteristics at $\alpha = 0^o$.

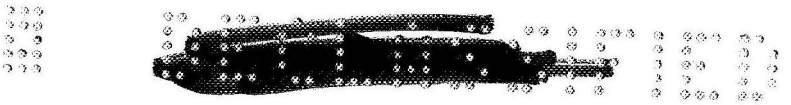

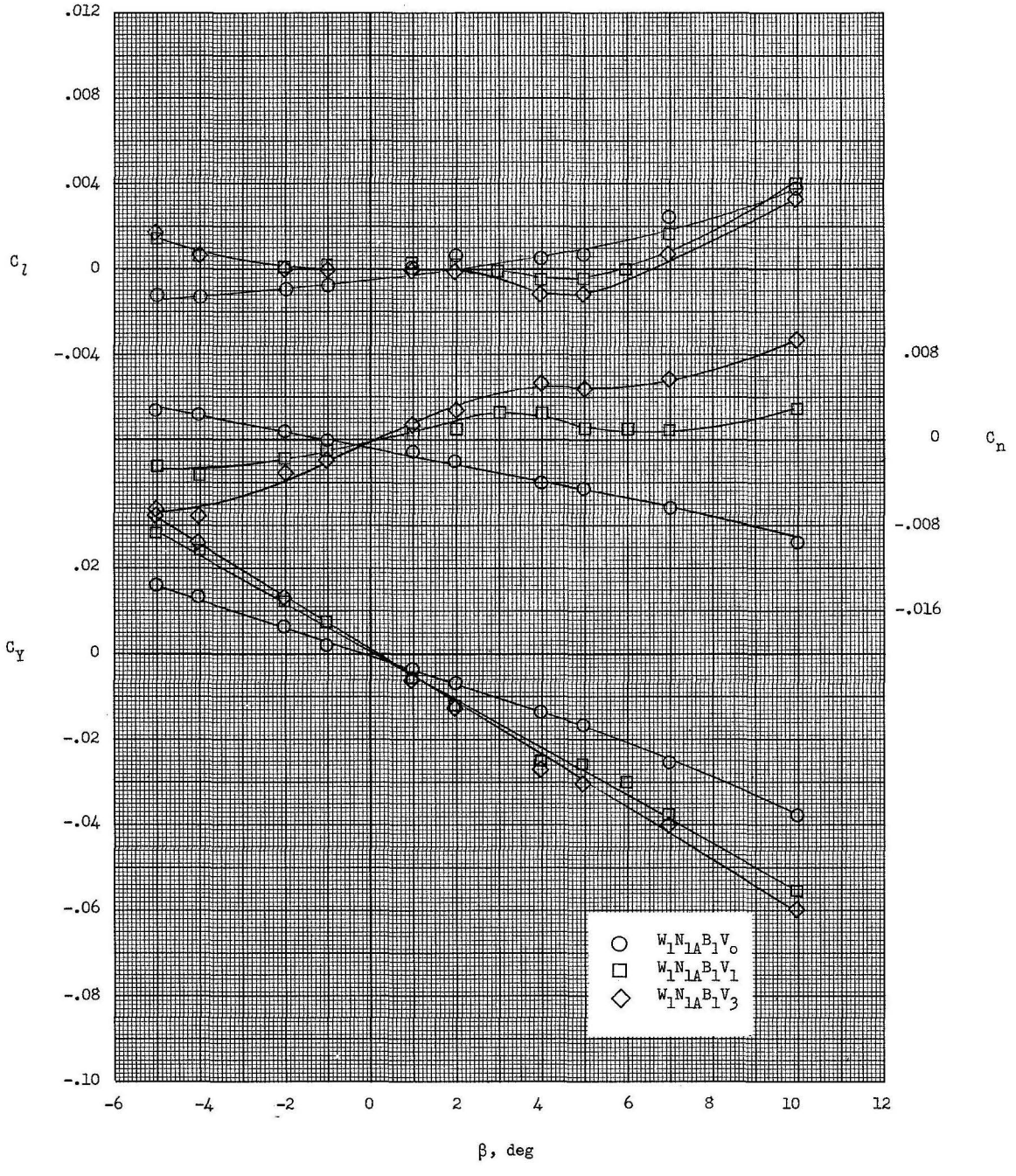

(b) Nose N_1; M = 17.8.

Figure 14.- Continued.

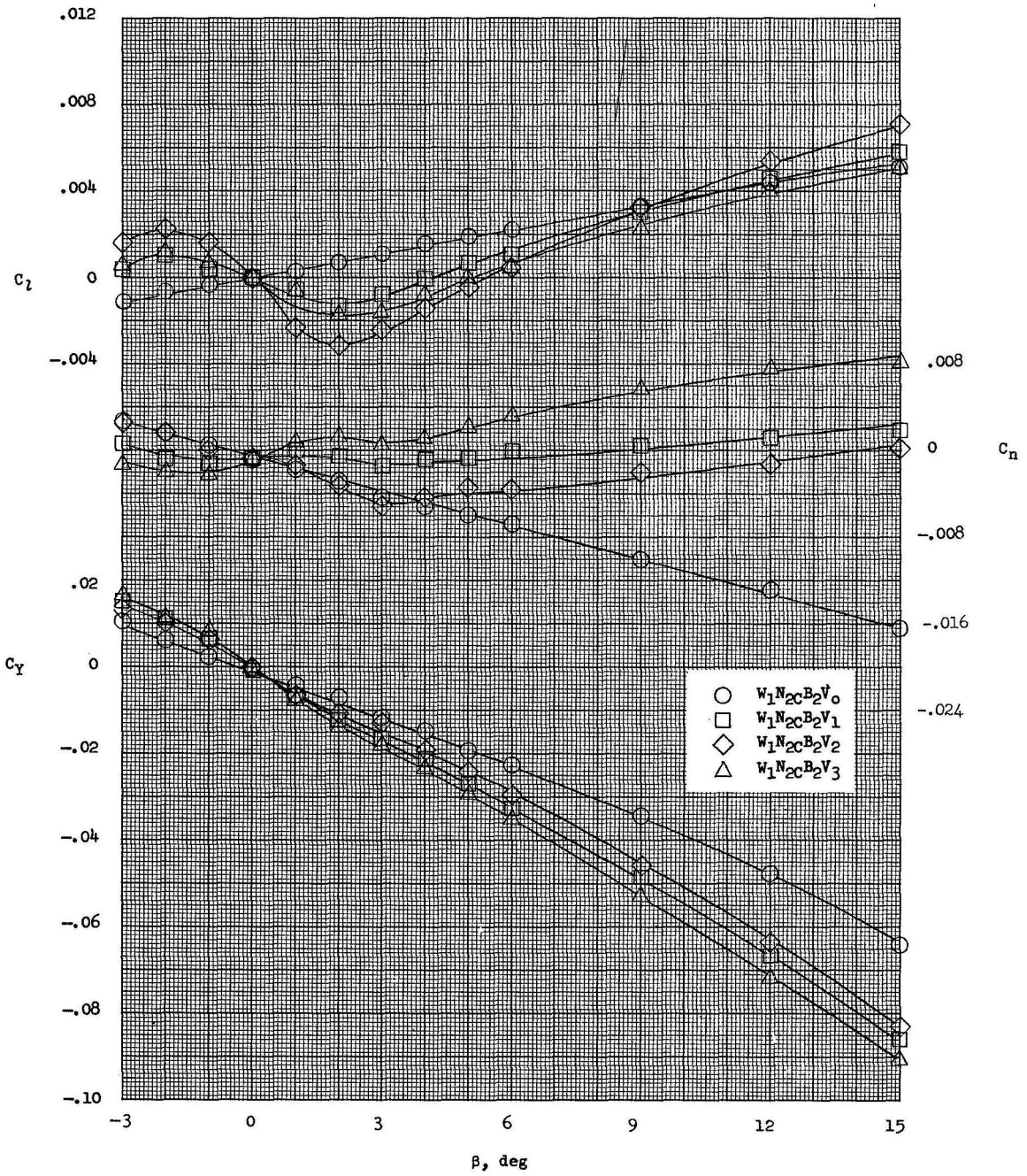

(c) Nose N_2; M = 9.6.

Figure 14.- Continued.

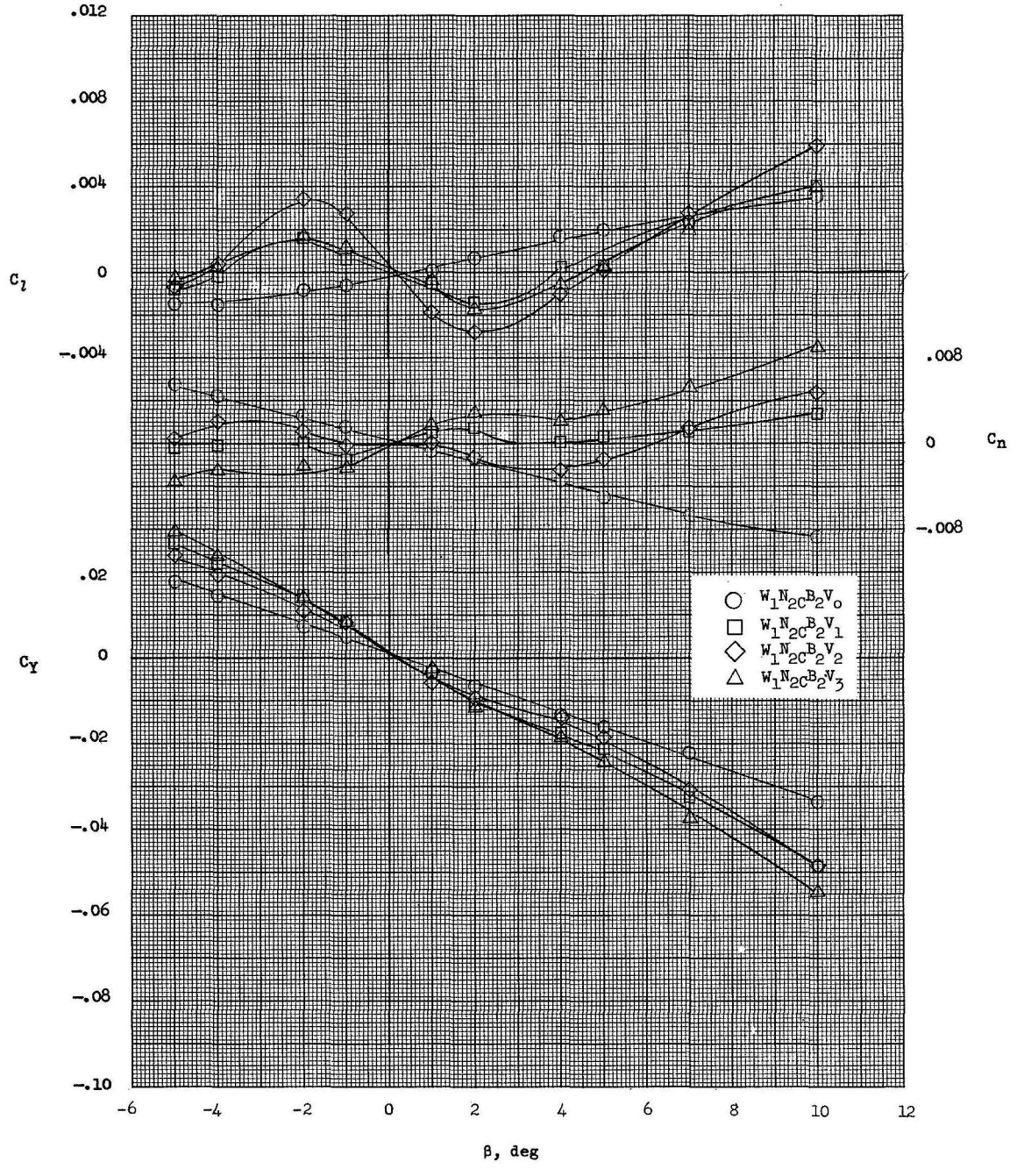

(d) Nose N_2; M = 17.8.

Figure 14.- Concluded.

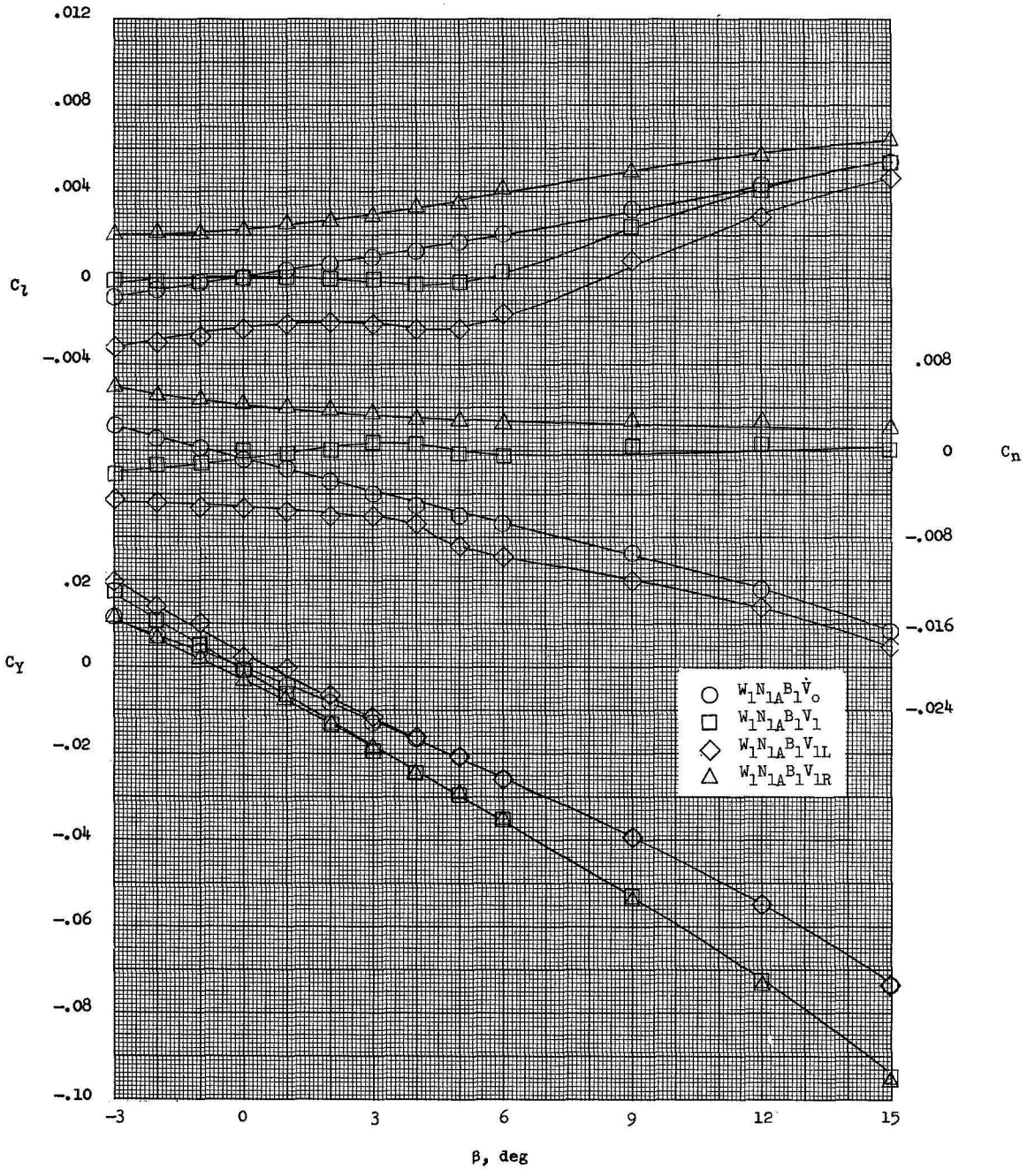

(a) Nose N_{1A}.

Figure 15.- Effect of V_1 vertical fins on directional and lateral aerodynamic characteristics at $\alpha = 0^o$. M = 9.6.

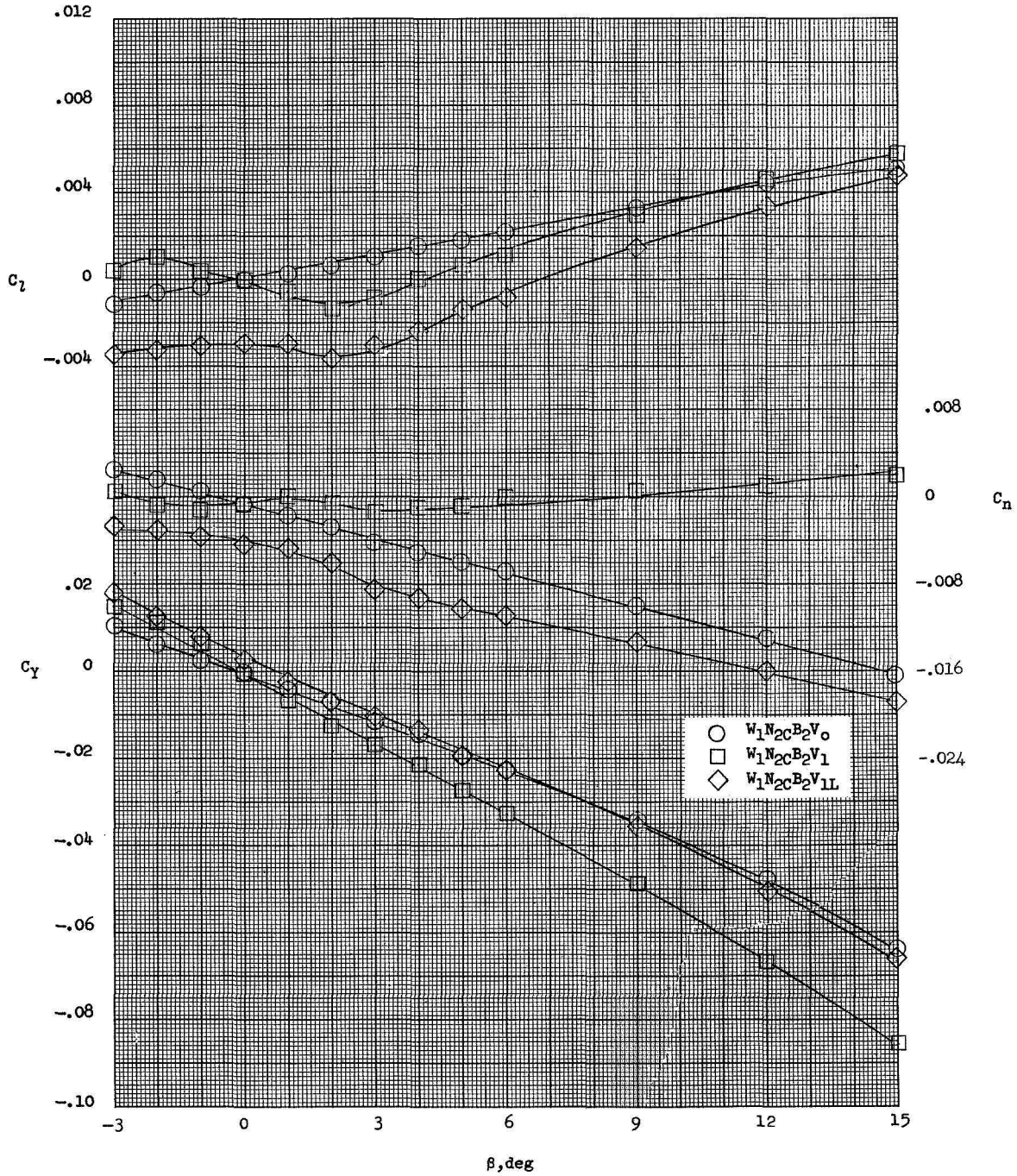

(b) Nose N_{2C}.

Figure 15.- Concluded.

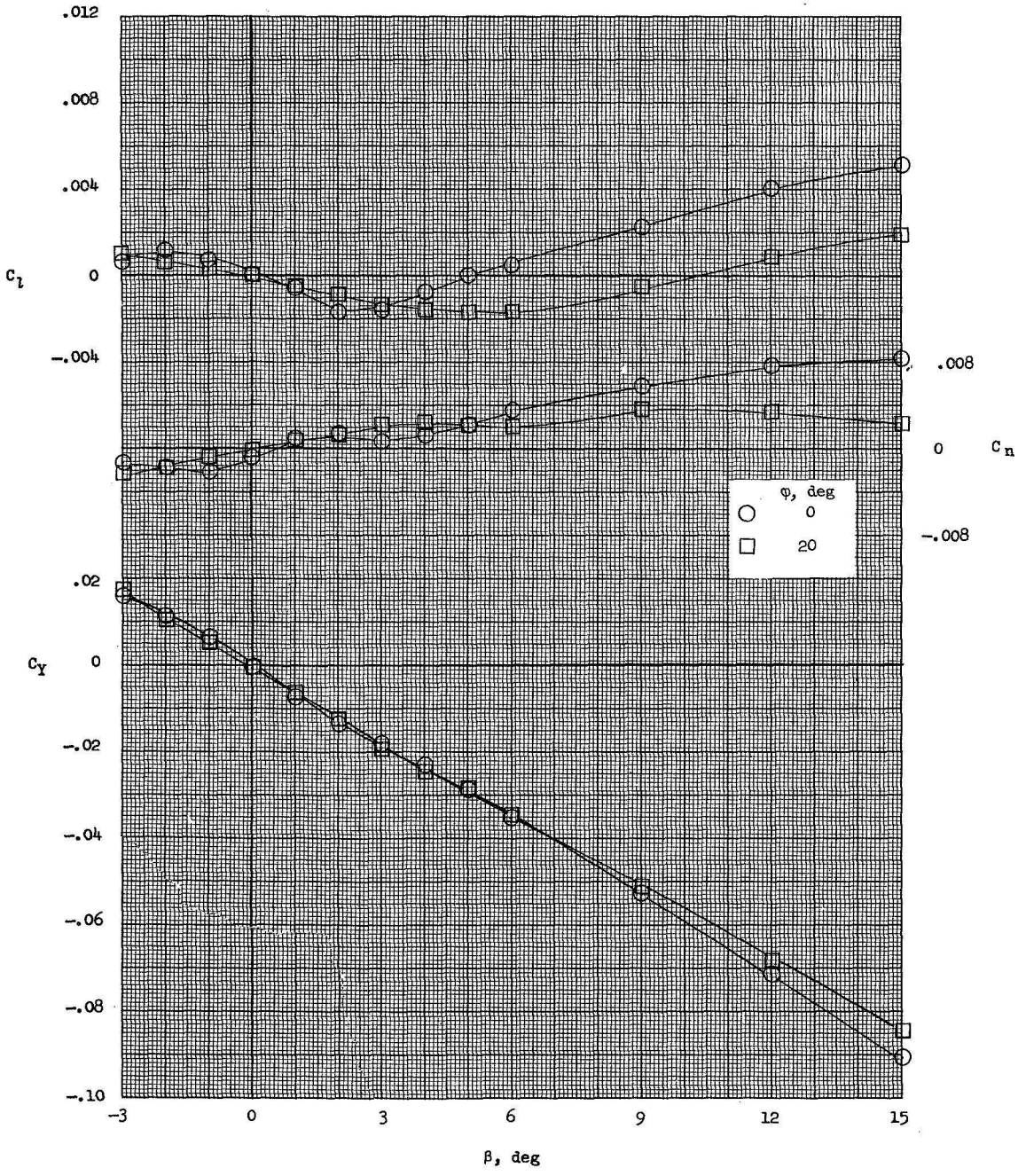

Figure 16.- Effect of vertical-fin rollout on directional and lateral aerodynamic characteristics of configuration $W_1N_{2C}B_2V_3$ at $\alpha = 0^\circ$. M = 9.6.

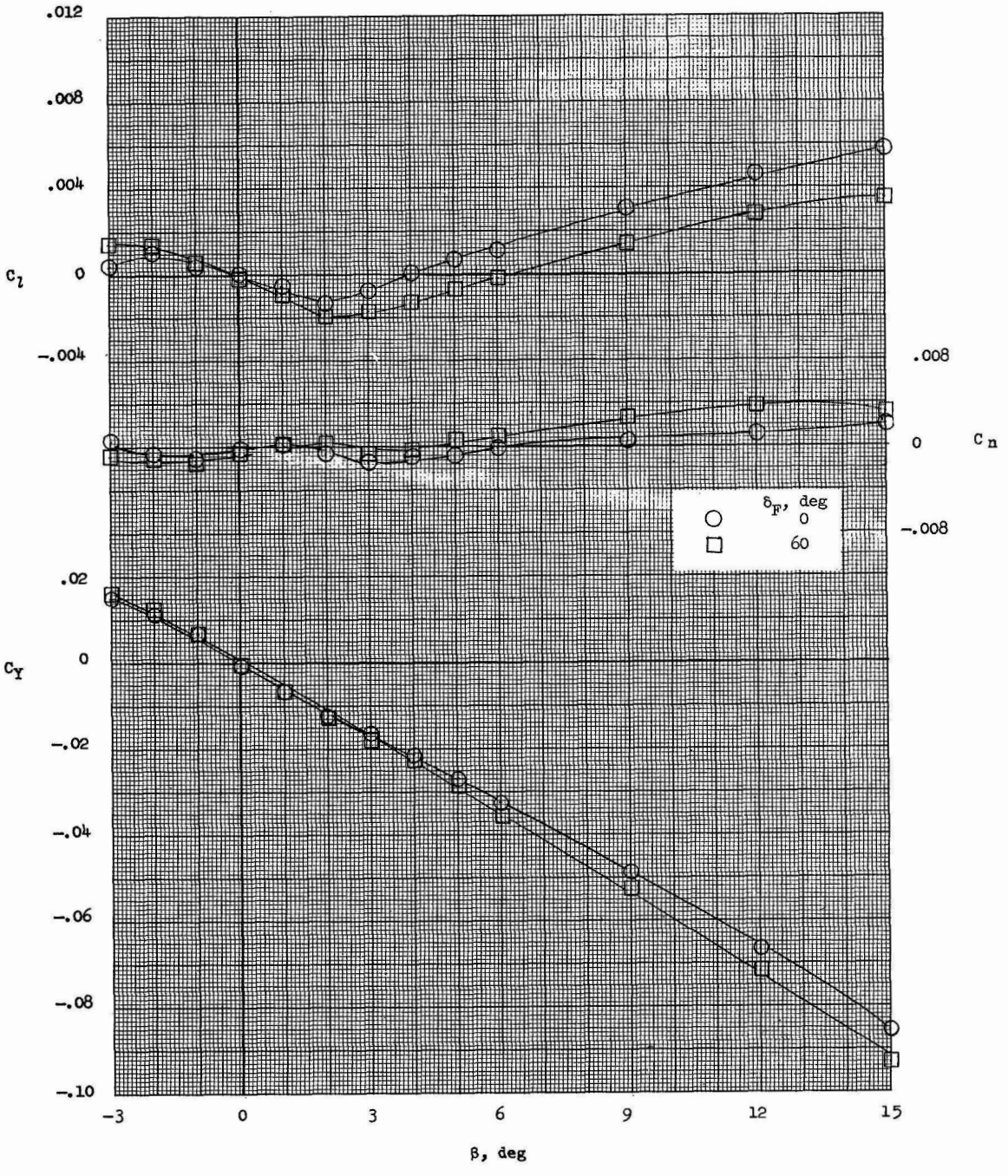

Figure 17.- Effect of body-flap deflection on directional and lateral aerodynamic characteristics of configuration $W_1N_{2C}B_2V_1F_1$ at $\alpha = 0^\circ$. M = 9.6.

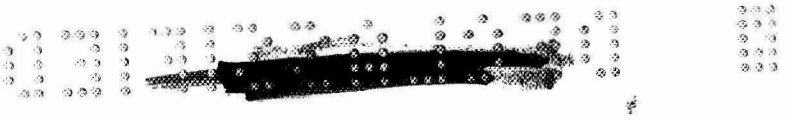

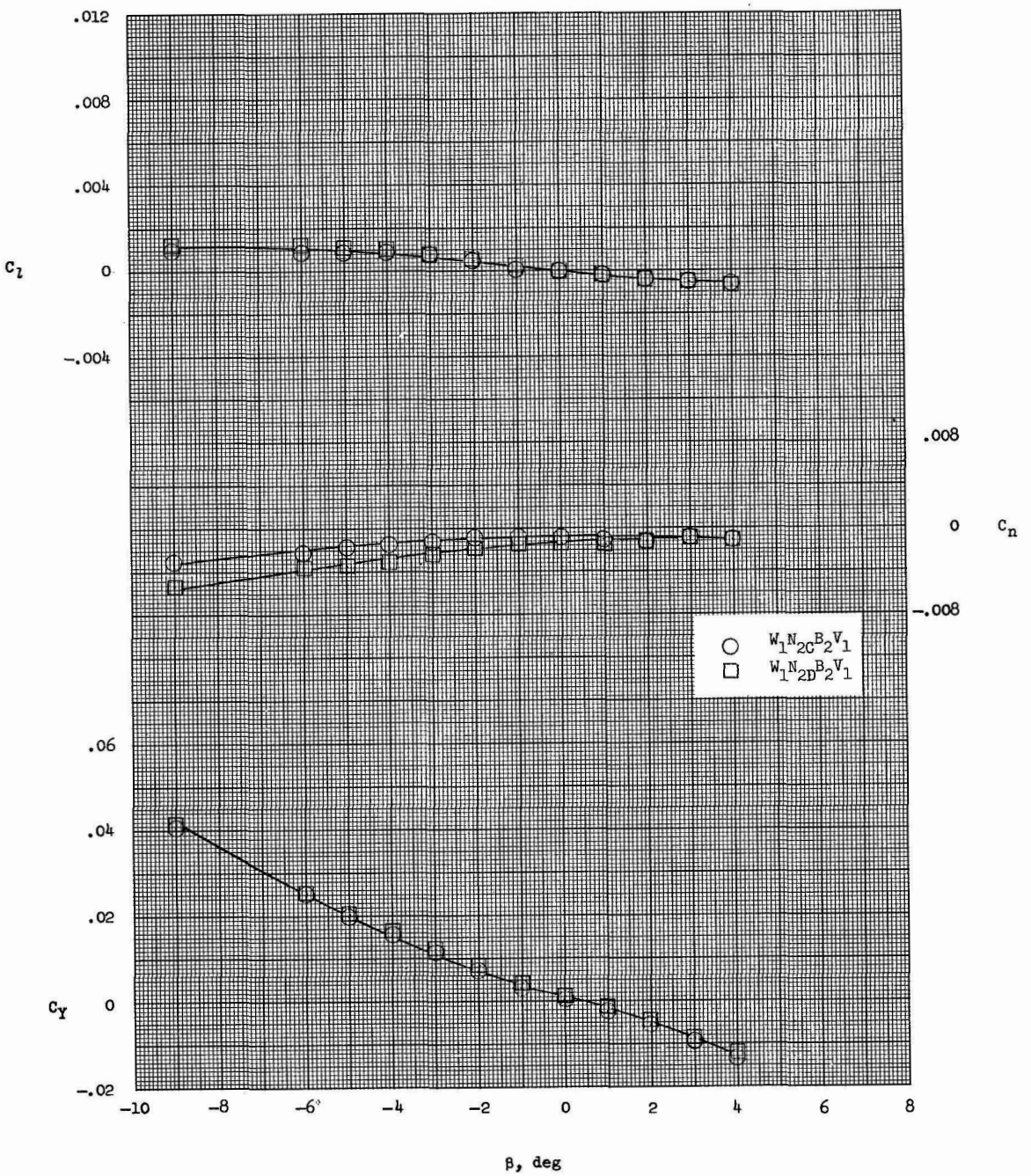

Figure 18.- Effects of nose shape on directional and lateral aerodynamic characteristics of nose N_2 at $\alpha = 10^o$. M = 9.6.

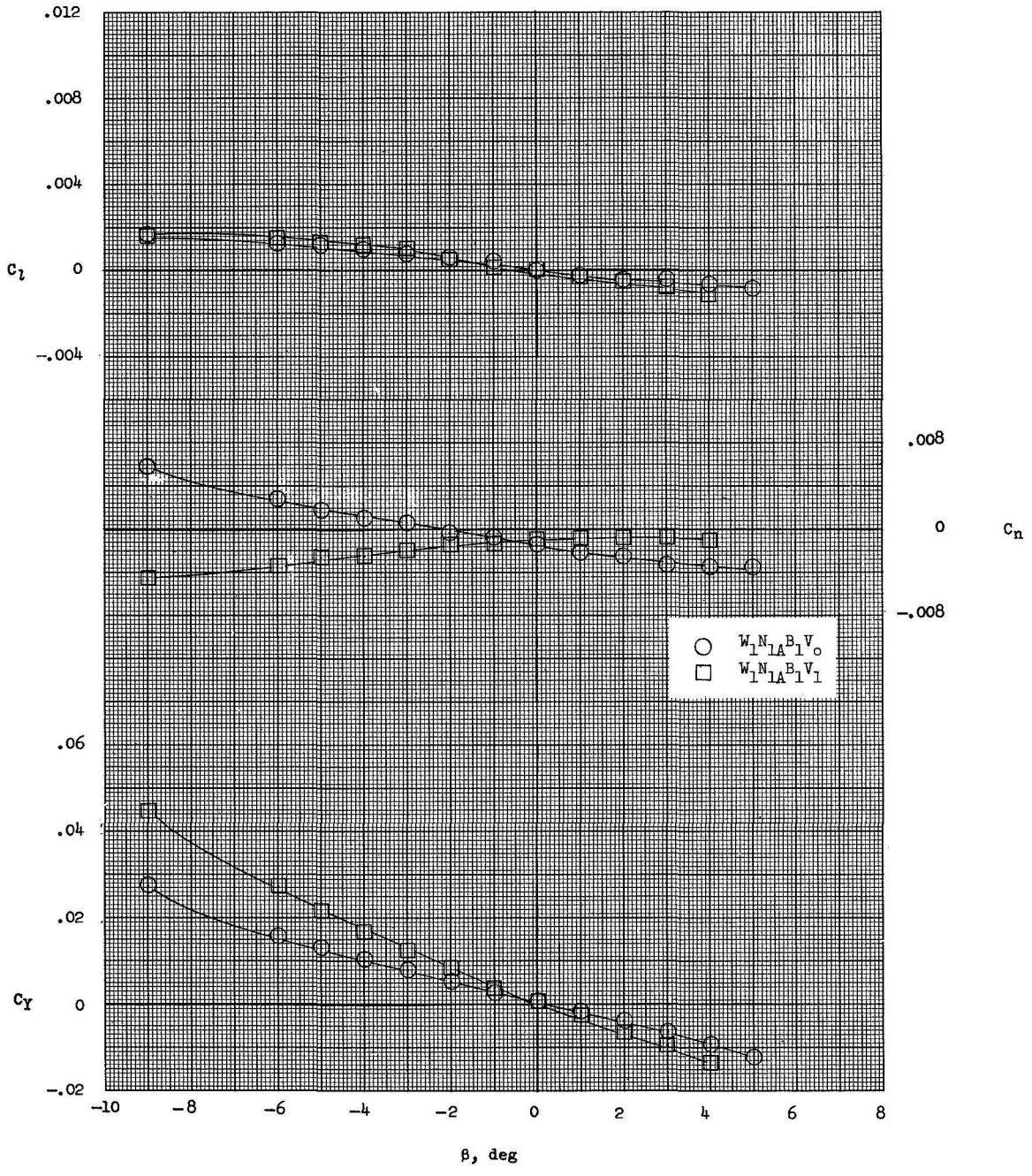

(a) Nose N_{1A}.

Figure 19.- Effects of vertical fins on directional and lateral aerodynamic characteristics at $\alpha = 10^{\circ}$. M = 9.6.

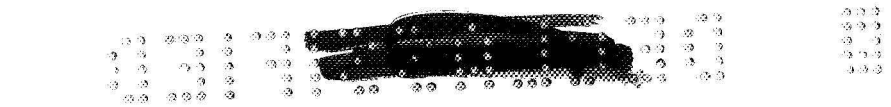

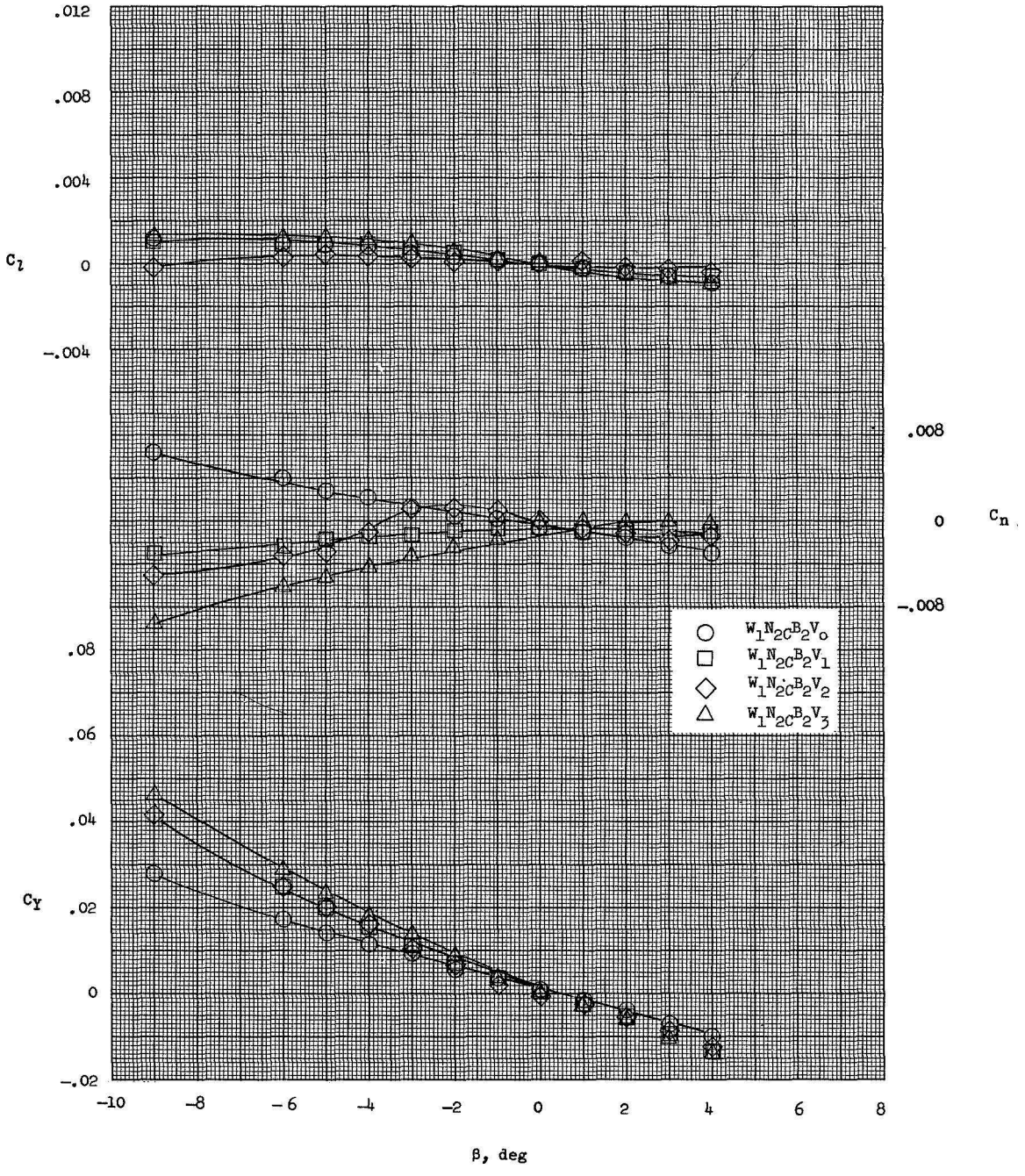

(b) Nose N_{2C}.

Figure 19.- Concluded.